Chapter 17
Axion Electrodynamics in Magnetoelectric Media

A. Martín-Ruiz, M. Cambiaso, and L. F. Urrutia

Abstract Topologically ordered media demand a new understanding of the emergent properties of quantum matter. This is a fundamental and technological feat. Topological insulators and Weyl semimetals are materials with topological order. Here we will focus on how these materials interact with sources of the electromagnetic field. We start from the effective field theory of Maxwell's electrodynamics extended by a so-called magnetoelectric term, namely axion electrodynamics and summarize some results we have found exploiting a Green's function approach to solve for the electromagnetic fields. Signals of the magnetolectric effect are minute compared with other electromagnetic responses, therefore precision measurements are required for its detection. Our formulation can be used for topological insulators and Weyl semimetals with planar, cylindrical and spherical geometries interacting with general charges, currents and boundary conditions. Our formulation is exemplified by: (i) the issue of Casimir effect involving a planar topological insulator, (ii) Vavilov-Cherenkov radiation produced in the forward- and backward-direction of a charged particle traversing a planar interface of two magnetoelectric media and (iii) the electromagnetic fields induced by a static electric charge near the surface of a Weyl semimetal. All three applications can yield observable signals that are within experimental sensitivities.

A. Martín-Ruiz · L. F. Urrutia (✉)
Instituto de Ciencias Nucleares, Universidad Nacional Autónoma de México, 04510 Ciudad de México, Mexico
e-mail: urrutia@nucleares.unam.mx

A. Martín-Ruiz
e-mail: alberto.martin@nucleares.unam.mx

M. Cambiaso
Universidad Andres Bello, Departamento de Ciencias Fisicas, Facultad de Ciencias Exactas, Avenida Republica 220, Santiago, Chile
e-mail: mcambiaso@unab.cl

E. Kamenetskii (ed.), *Chirality, Magnetism and Magnetoelectricity*,
Topics in Applied Physics 138,
https://doi.org/10.1007/978-3-030-62844-4_17

17.1 Introduction

Classical and quantum electrodynamics summarize all our understanding of the interaction between matter and radiation. Although these topics have been profusely studied in many different areas since their early discoveries, still today they constitute a fruitful research discipline and an excellent arena with potential for new discoveries. This is specially true when precision measurements are at hand and also when new materials come into play whose novel properties, of ultimate quantum origin, result in new possible forms of interaction between light and such materials. That is the case with topological insulators, as well as other materials with topological order.

Interestingly enough, the interaction between matter characterized by topological order and external electromagnetic fields can be described by an extension of Maxwell's theory. In fact, in electrodynamics there is the possibility of writing two quadratic gauge and Lorentz invariant terms: the first one is the usual electromagnetic density $\mathcal{L}_{\text{EM}} = (\mathbf{E}^2 - \mathbf{B}^2)/8\pi$ which yields Maxwell's equations, and the second one is the magnetoelectric term $\mathcal{L}_\theta = \theta\, \mathbf{E} \cdot \mathbf{B}$, where θ is a coupling field usually termed the axion angle.

Many of the interesting properties of the latter can be recognized from its covariant form $\mathcal{L}_\theta = -(\theta/8)\epsilon^{\mu\nu\rho\lambda} F_{\mu\nu} F_{\rho\lambda}$, where $\epsilon^{\mu\nu\rho\lambda}$ is the Levi-Civita symbol and $F_{\mu\nu} = \partial_\mu A_\nu - \partial_\nu A_\mu$ is the electromagnetic field strength written in terms of the connection A_μ. When θ is globally constant, the θ-term is a total derivative and has no effect on Maxwell's equations. This property, together with its invariance under continuous changes in the connection A_μ, qualify $\mathcal{P} = -(1/8)\epsilon^{\mu\nu\rho\lambda} F_{\mu\nu} F_{\rho\lambda}$ to be a topological invariant. Actually, $\mathcal{P}$ is the simplest example of a Pontryagin density [1], corresponding to the abelian group $U(1)$. This structure, together with its generalization to nonabelian groups, has been relevant in diverse topics in high-energy physics such as anomalies [2], the strong CP problem [3], topological field theories [4] and axions [5], for example.

It is interesting to recall that the coupling to a Pontryagin density has a long story in the development of Yang-Mills theories, with its origin dating back to a problem arising because the axial symmetry of the QCD Lagrangian, in the massless limit, would imply the existence of low mass nucleons with odd parity, which are not found in nature [6]. The alternative realization of this symmetry in the spontaneously broken mode is not possible either because the three lighter mesons in the spectrum (the pions) do not match the required four pseudo Goldstone bosons. The absence of a fourth pseudoscalar meson with a mass similar to that of the pions is what is known as the $U(1)_A$ problem. A solution was proposed in [7, 8] grounded in a more detailed study of the structure of the vacuum in a Yang-Mills theory, which introduces a superposition of topologically nonequivalent vacua as the true ground state of the system: the θ vacuum. This superposition eliminates the $U(1)_A$ problem but requires the CP violating coupling of the θ-vacuum to the non-abelian Pontryagin density in the QCD Lagrangian. Unfortunately, this addition generates a new problem. In particular, the resulting effective pion-nucleon interaction predicts an electric dipole moment for the neutron given by $d_n \sim 3.2 \times 10^{-16}\theta$ e cm. Comparison with the

experimental value $(d_n)_{\text{exp}} < 3 \times 10^{-26}$ e cm produces the naturalness problem: why should $\theta \sim 10^{-10}$ be so small. This is known as the strong CP problem. A solution was proposed in [9, 10] through the introduction of a new field, the axion $a(x)$, and a new symmetry $U(1)_{\text{PQ}}$ realized again in the spontaneously broken mode. The vacuum expectation value of $a(x)$ can be chosen to cancel the previous CP violating term, but a new pseudo Goldstone boson must appear. Estimations of the coupling constant and mass of this new particle reveal extremely low values, thus making its detection very difficult. The abelian sector of the axion coupling in the QCD Lagrangian, $\mathcal{L}_{a\gamma\gamma} = -g_{a\gamma\gamma} a\, \mathbf{E}\cdot\mathbf{B}$, was proposed in [11] as a possibility to detect the axion through its coupling with strong electromagnetic fields available in the laboratory. The addition of this term to the usual electromagnetic Lagrangian, gives rise to what is now known as axion electrodynamics. Recently the axion is considered as a candidate to describe dark matter. Reference [5] contains a recent review of axion physics, including the efforts made towards its detection.

Another subject related to the θ-coupling is the photon sector of the Standard Model Extension (SME), designed to study possible violations of the Lorentz and CPT symmetries [12–14]. There one considers the effective couplings $(k_F)_{\kappa\lambda\mu\nu} F^{\kappa\lambda} F^{\mu\nu}$ and $(k_{AF})^{\kappa} \epsilon_{\kappa\lambda\mu\nu} A^{\lambda} F^{\mu\nu}$ where the constant tensors $(k_F)_{\kappa\lambda\mu\nu}$ and $(k_{AF})^{\kappa}$ define fixed directions in spacetime that break Lorentz symmetry. An alternative way to perform this breaking is by choosing spacetime dependent coupling parameters [15], like $(k_F)_{\kappa\lambda\mu\nu} = \theta(x)\epsilon_{\kappa\lambda\mu\nu}$ and $(k_{AF})_{\kappa} = \partial_{\kappa}\theta(x)$, for example. Both cases yield a version of the axion coupling described previously which can be used as effective theories with real Lorentz symmetry breaking in matter. The point of this comment is to observe that many of the techniques and of the numerous high-precision experiments proposed to test Lorentz symmetry breaking could adapt to the case of matter-photon interaction.

Recently, an important additional application of the Pontryagin extended electrodynamics has been highlighted in condensed matter physics, where a non-dynamical axion angle θ provides an effective field theory describing the electromagnetic response of some materials such as (i) magnetoelectric media [16, 17], (ii) metamaterials when θ is a purely complex function [18], (iii) topological insulators (TIs) when $\theta = (2n+1)\pi$, with n integer [19–22] and (iv) Weyl semimetals (WSM) when $\theta(\mathbf{x}, t) = 2\mathbf{b}\cdot\mathbf{x} - 2b_0 t$, where $\mathbf{b}$ is the separation in momentum space between the Weyl nodes and b_0 is their separation in energy [23]. Lately, the study of topological insulating and Weyl semimetal phases, either from a theoretical or an experimental perspective has been actively pursued [22–24].

We will devote this chapter to the study of the interaction between magnetoelectric media and the electromagnetic field. To do so we will employ field theoretic techniques predicated on the aforementioned model Lagrangian of Maxwell's theory extended by the magnetoelectric term. The chapter is organized as follows. In Sect. 17.2 we present the general framework of electrodynamics in media characterized by a parameter θ (to be called a θ-medium) and review some of the most important features of magnetoelectric media regarding their electromagnetic properties. Section 17.3 contains a summary of our generalized Green's function method to construct the corresponding electromagnetic fields produced by charges, currents

and boundary conditions in systems satisfying the following coordinate conditions: (i) the coordinates can be chosen such that the interface between two media, with different θ, is defined by setting to a constant only one of coordinates and (ii) the Laplacian is separable in such coordinates. At the end of this section the particularly simple case of planar symmetry is discussed. There the reader is referred to the analogous extensions to cylindrical and spherical coordinates. As a specific application of our methods to the case of a planar interface, the Casimir effect between two metallic plates with a topological insulator between them is considered in Sect. 17.4. In Sect. 17.5, we study the problem of Vavilov-Cherenkov radiation produced by an electric charge propagating perpendicularly to the planar interface between two different magnetoelectric media to find that, besides the usual forward-directed radiation, there is a backward-directed emission of radiation, a so-called reversed Vavilov-Cherenkov radiation (RVCR), solely due to the magnetoelectric nature of the media. As yet another application, in Sect. 17.6 we show how a static electric charge induces unexpected electromagnetic fields when placed near the surface of a Weyl semimetal and provide two experimental proposals, feasible for present-day sensitivities, that could be performed to measure the effects associated with the topological character of the WSM. Finally in Sect. 17.7 we present some concluding remarks, provide a summary of important results and highlight the benefits of our approach for solving the electromagnetic response of magnetoelectric media.

Our conventions are taken from [25], where $F_{\mu\nu} = \partial_\mu A_\nu - \partial_\nu A_\mu$, $\tilde{F}^{\mu\nu} = \epsilon^{\mu\nu\alpha\beta} F_{\alpha\beta}/2$, $F^{i0} = E^i$, $F^{ij} = -\epsilon^{ijk} B^k$ and $\tilde{F}^{i0} = B^i$, $\tilde{F}^{ij} = \epsilon^{ijk} E^k$. Also $\mathbf{V} = (V^i) = (V_x, V_y, V_z)$ for any vector $\mathbf{V}$. The metric is $(+, -, -, -)$ and $\epsilon^{0123} = +1 = \epsilon^{123}$.

17.2 Nondynamical Axion Electrodynamics

In this section we discuss the basic features arising from adding to Maxwell's electrodynamics the coupling of the abelian Pontryagin density to a pseudoscalar field $\theta(x)$, leading to a theory that we call θ-electrodynamics (θ-ED), retaining the name of axion-electrodynamics for the case where the axion field θ becomes dynamical. We call the parameter $\theta(x)$ the magnetoelectric polarizability (MEP) of the medium, which we consider in the same footing as its permittivity ε and permeability μ. The nature of the MEP depends on the type of magnetoelectric material under consideration and it is ultimately related to the magnetic symmetries of the substance [26, 27] and/or to the properties of its band structure [19–21]. It can be calculated from a Kubo-type response formula, once a microscopic model Hamiltonian for the material is adopted. The permittivity tensor ϵ is usually understood by the Drude-Lorentz type of single resonance oscillator model [28].

Magnetoelectric media [16, 17] are naturally existing materials like antiferromagnets [30], topological insulators (TIs) [19–22] and Weyl semimetals [23, 24], for example. Leaving aside the remarkable microscopic properties of different magnetoelectric media, we will concentrate on θ-ED as the effective macroscopic theory

describing the electromagnetic response in the case of linear, isotropic and homogeneous magnetoelectrics. Let us start from the general formulation of electrodynamics in a material medium according to the Maxwell equations

$$\nabla \cdot \mathbf{D} = 4\pi\rho, \quad \nabla \cdot \mathbf{B} = 0, \quad \nabla \times \mathbf{E} + \frac{1}{c}\frac{\partial \mathbf{B}}{\partial t} = 0, \quad \nabla \times \mathbf{H} - \frac{1}{c}\frac{\partial \mathbf{D}}{\partial t} = \frac{4\pi}{c}\mathbf{J}, \tag{17.1}$$

together with the Lorentz force

$$\mathbf{F}_L = q\left(\mathbf{E} + \frac{\mathbf{v}}{c} \times \mathbf{B}\right). \tag{17.2}$$

The characterization of a specific media is given by the constitutive relations which define the displacement $\mathbf{D}$ and the magnetic field $\mathbf{H}$ in terms of the electric field $\mathbf{E}$ and the magnetic induction $\mathbf{B}$, which are the fundamental fields that define the electromagnetic potentials according to the homogeneous equations in (17.1) [25].

The constitutive relations depend on the nature of the material and usually have the form $\mathbf{D} = \mathbf{D}(\mathbf{E}, \mathbf{B})$ and $\mathbf{H} = \mathbf{H}(\mathbf{E}, \mathbf{B})$. For example, in linear nonmagnetoelectric media they are $D_i = \varepsilon_{ij} E_j$ y $B_i = \mu_{ij} H_j$, where ε_{ij} is the permittivity and μ_{ij} is the permeability tensors, respectively, which can depend on the position and time. For isotropic and homogeneous materials $\varepsilon_{ij} = \varepsilon\delta_{ij}$ and $\mu_{ij} = \mu\delta_{ij}$, with ε and μ constants. In the case of magnetoelectrics we will consider media described by the following constitutive relations

$$\mathbf{D} = \varepsilon\mathbf{E} - \frac{\theta\alpha}{\pi}\mathbf{B}, \qquad \mathbf{H} = \frac{1}{\mu}\mathbf{B} + \frac{\theta\alpha}{\pi}\mathbf{E}, \tag{17.3}$$

where $\alpha = e^2/\hbar c \simeq 1/137$ is the fine-structure constant and the MEP θ is an additional parameter of the medium. The extension of these constitutive relations to the anisotropic case, for the optical properties of the material (ε and μ) is direct and for the MEP θ is also possible.

Substituting them in (17.1), we obtain the following modified non-homogeneous Maxwell equations

$$\nabla \cdot (\varepsilon\mathbf{E}) = 4\pi\rho + \frac{\alpha}{\pi}\nabla\theta \cdot \mathbf{B}, \quad \nabla \times (\mathbf{B}/\mu) - \frac{1}{c}\frac{\partial(\varepsilon\mathbf{E})}{\partial t} = \frac{4\pi}{c}\mathbf{J} - \frac{\alpha}{\pi}\nabla\theta \times \mathbf{E} - \frac{1}{c}\frac{\alpha}{\pi}\frac{\partial\theta}{\partial t}\mathbf{B}. \tag{17.4}$$

We observe that the above equations can be derived from the usual Maxwell action extended by the coupling of the abelian Pontryagin density $\mathcal{P}$ to a non-dynamical axion field $\theta(\mathbf{x}, t)$

$$S[\Phi, \mathbf{A}] = \int dt\, d^3\mathbf{x} \left[\frac{1}{8\pi}\left(\varepsilon\mathbf{E}^2 - \frac{1}{\mu}\mathbf{B}^2\right) - \frac{\alpha}{4\pi^2}\theta(\mathbf{x}, t)\,\mathbf{E} \cdot \mathbf{B} - \rho\Phi + \frac{1}{c}\mathbf{J} \cdot \mathbf{A}\right]. \tag{17.5}$$

The electromagnetic fields **E** and **B** are expressed in terms of the electromagnetic potentials Φ and **A** as

$$\mathbf{E} = -\frac{1}{c}\frac{\partial \mathbf{A}}{\partial t} - \nabla\Phi, \qquad \mathbf{B} = \nabla \times \mathbf{A}, \tag{17.6}$$

which solve the homogeneous equations in (17.1). An important consequence of (17.4) is the so-called magnetoelectric effect (MEE), summarized in the appearance of the following effective field dependent charge and current densities

$$\rho_\theta = \frac{\alpha}{4\pi^2}\nabla\theta \cdot \mathbf{B}, \qquad \mathbf{J}_\theta = -\frac{c\alpha}{4\pi^2}\nabla\theta \times \mathbf{E} - \frac{\alpha}{4\pi^2}\frac{\partial\theta}{\partial t}\mathbf{B}, \tag{17.7}$$

evidencing the ability of the magnetic (electric) fields to produce charge (current) densities, respectively. This effect is one of the most remarkable physical consequences of the additional θ coupling. It was predicted in [26] and subsequently observed in [30]. For an updated review of the MEE see, for example, [31]. A universal topological magnetoelectric effect has recently been measured in TIs [32]. Many additional consequences of the MEE have been highlighted using different approaches. For example, electric charges close to the interface between two θ-media induce image magnetic monopoles (and vice versa) [33–36]. Also, the propagation of electromagnetic waves across a θ-boundary have been studied finding that a non trivial Faraday rotation of the polarizations appears [29, 34, 35, 37]. The shifting of the spectral lines in hydrogen-like ions placed in front of a planar TI, as well as the modifications to the Casimir Polder potential in the non-retarded approximation were studied in [38]. The classical dynamics of a Rydberg hydrogen atom near a planar TI has also been investigated [39].

We observe that the dynamical modifications in (17.4) depend on the spatial and temporal gradients of the MEP, as required because the Pontryagin density $\mathcal{P}$ is a total derivative. In this way, the coupling with θ does not affect the equations of motion when the MEP is globally constant. The explicit dependence on θ, instead of $\partial_\mu\theta$, of the constitutive relations may erroneously induce the belief that a globally constant θ could produce dynamical effects. Nevertheless, from this perspective one would identify additional polarization $\mathbf{P}_\theta = -\sigma\mathbf{B}$ and magnetization $\mathbf{M}_\theta = -\sigma\mathbf{E}$ with $\sigma = \theta\alpha/4\pi^2$. When θ is constant, the calculation of the effective sources

$$\rho_{\text{eff}} = \nabla \cdot \mathbf{P}_\theta = \sigma\nabla \cdot \mathbf{B}, \qquad \mathbf{J}_{\text{eff}} = \frac{1}{c}\frac{\partial \mathbf{P}_\theta}{\partial t} + \nabla \times \mathbf{M}_\theta = -\sigma\left(\frac{1}{c}\frac{\partial \mathbf{B}}{\partial t} + \nabla \times \mathbf{E}\right), \tag{17.8}$$

yields identically zero due to the homogeneous Maxwell equations.

17.3 The Green Function Approach to the Electromagnetic Response of Linear Isotropic Homogeneous Magnetolectric Media

The knowledge of the Green function (GF) of an electromagnetic system allows the calculation of its response to arbitrary external sources, providing a definite starting point for the algebraic or numerical approximations which are required in most cases. This method supersedes the image approach, frequently used in the literature, which is appealing for interpreting results in terms of the superposition of images of charges and currents. Nevertheless, it requires a good amount of educated guesses which are far from obvious in many interesting cases. We will focus on calculating the GFs for the cases when materials with piecewise constant MEP's exhibit planar, cylindrical and spherical symmetries. Certainly one could solve for the electric and magnetic fields from the modified Maxwell equations together with the boundary conditions, however, just as in ordinary electrodynamics, there might be occasions where information about the sources is unknown and rather we are provided with data of the 4-potential at some given boundaries. In these cases, the GF method provides the general solution to such boundary-value problem (Dirichlet or Neumann) for arbitrary sources.

As an important class of magnetoelectric media with constant MEP we single out TIs, which serve to illustrate some of the phenomena discussed. Three dimensional TIs are a class of topological materials that can host conducting helical surface states each having the dispersion relation of a non-degenerate Dirac cone with a crossing point at/close to the Fermi level. Nevertheless, TIs behave as insulators in the bulk with a finite energy gap. The surface state is further topologically protected by time-reversal symmetry and/or inversion symmetry, coupled with spin-momentum locking properties. The latter means that the spin orientation of the electrons on the surface Dirac cone is always locked perpendicularly to their momentum. A distinguishing feature of 3D TIs among magnetoelectrics, is that the MEP θ is of topological nature and arises from the bulk band structure. It is given by a non-Abelian Berry flux over the Brillouin zone [19]. For 3D time reversal invariant insulators in a manifold without boundaries there are only two possibilities: $\theta = 0$ for normal insulators and $\theta = \pi$ for TIs. In order to continuously connect both classes of insulators, time reversal invariance should be broken at the interface. This can be achieved, for example, by depositing a thin magnetic coating of a few nanometers at the interface. According to the specific nature of the coating, the MEP of the TI will be modified to $\theta = \pi + 2n\pi$, where n is an integer [40].

From a macroscopic perspective we consider TIs as a class of magnetoelectric media described by θ-ED and characterized by the choice of a constant MEP θ. To illustrate the calculation of the GF it will be enough to consider the simplest case where the $(3 + 1)$ dimensional spacetime $\mathcal{M}$ can be split in such a way that $\mathcal{M} = \mathcal{U} \times \mathbb{R}$, where $\mathcal{U}$ is a three-dimensional manifold and $\mathbb{R}$ is the temporal axis. Moreover, the space $\mathcal{U}$ is partitioned in two region $\mathcal{U}_1$ and $\mathcal{U}_2$, such that $\mathcal{U}_1$ and $\mathcal{U}_2$ have a two-dimensional common interface Σ. In this way $\mathcal{U} = \mathcal{U}_1 \cup \mathcal{U}_2$ and

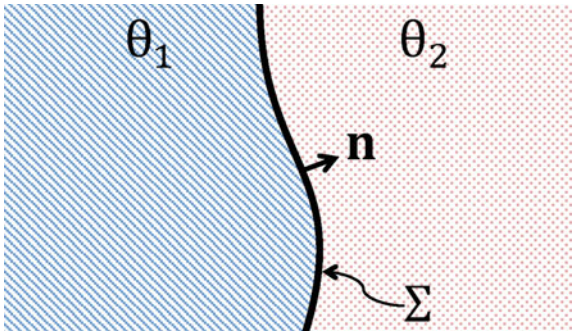

Fig. 17.1 Region over which the electromagnetic field theory is defined, (adapted from [43])

$\Sigma = \mathcal{U}_1 \cap \mathcal{U}_2$, as shown in the Fig. 17.1. Also we assume that the MEP θ is piecewise constant taking the values $\theta = \theta_1$ in the region $\mathcal{U}_1$ and $\theta = \theta_2$ in the region $\mathcal{U}_2$, which is expressed by the characteristic function

$$\theta(\mathbf{x}) = \begin{cases} \theta_1 & , \quad \mathbf{x} \in \mathcal{U}_1 \\ \theta_2 & , \quad \mathbf{x} \in \mathcal{U}_2 \end{cases} . \tag{17.9}$$

The interface Σ is parametrized by a function $F_\Sigma(\mathbf{x}) = 0$, which yields $n_\mu = (0, \mathbf{n}) = \partial_\mu F_\Sigma(\mathbf{x})$, as the normal vector to Σ which is external to the region $\mathcal{U}_1$. In this setup, the action S_θ, corresponding to the second term on the right-hand side of (17.5), is no longer a total derivative and the modified Maxwell equations (17.4) acquire field dependent effective charges and currents with support only at the interface (in the following we set $c = 1$)

$$\nabla \cdot (\epsilon \mathbf{E}) = \tilde{\theta}\delta\left(F_\Sigma(\mathbf{x})\right) \mathbf{B} \cdot \mathbf{n} + 4\pi\rho, \tag{17.10}$$

$$\nabla \times \left(\mathbf{B}/\mu\right) - \frac{\partial(\epsilon \mathbf{E})}{\partial t} = \tilde{\theta}\delta\left(F_\Sigma(\mathbf{x})\right) \mathbf{E} \times \mathbf{n} + 4\pi \mathbf{J}. \tag{17.11}$$

Here $\mathbf{n}$ is the vector normal to Σ external to the region $\mathcal{U}_1$ and $\tilde{\theta} = \alpha\left(\theta_1 - \theta_2\right)/\pi$. Equations (17.10)–(17.11) show that in the bulk regions $\mathcal{U}_{1,2}$ we recover the usual Maxwell equations. The MEE shows up again in (17.10)–(17.11) and the realization of such effect that can provide a way to measure the MEP of a medium, is one of the main goals in the research related to TIs.

In the following we restrict ourselves to contributions of free sources only outside the interface Σ, with no additional boundary conditions (BCs) besides those required at Σ. Assuming that the temporal derivatives of the fields are finite in the neighbourhood of the interface, the field equations (17.10) and (17.11) yield the following boundary conditions

$$\Delta\mathbf{E} \cdot \mathbf{n}\big|_\Sigma = \tilde{\theta}\mathbf{B} \cdot \mathbf{n}\big|_\Sigma, \quad \Delta\mathbf{B} \times \mathbf{n}\big|_\Sigma = -\tilde{\theta}\mathbf{E} \times \mathbf{n}\big|_\Sigma, \tag{17.12}$$

$$\Delta\mathbf{B} \cdot \mathbf{n}\big|_\Sigma = 0, \quad \Delta\mathbf{E} \times \mathbf{n}\big|_\Sigma = 0. \tag{17.13}$$

The notation $\Delta \mathbf{V}_i\big|_\Sigma$ stands for the discontinuity of the i component of the vector $\mathbf{V}$ through the interface Σ, while $\mathbf{V}_j\big|_\Sigma$ indicates the continuous value of the j component evaluated at Σ. The boundary conditions in (17.13) imply that the members of the right hand side in (17.12) are correctly defined, representing field dependent charge densities and surface currents respectively. Again, the magnetoelectric effect is manifest in the boundary conditions (17.12). In order to emphasize the effects of the topological coupling we consider the simplest media having $\theta_1 \neq \theta_2$, but with $\varepsilon = 1$ and $\mu = 1$.

At this stage it is convenient to go back to the four dimensional notation: $A^\mu = (\Phi, \mathbf{A})$, $F_{\mu\nu} = \partial_\mu A_\nu - \partial_\nu A_\mu$, $\tilde{F}^{\mu\nu} = \frac{1}{2}\epsilon^{\mu\nu\alpha\beta}F_{\alpha\beta}$, $j^\mu = (\rho, \mathbf{J})$. In this way, the
inhomogeneous Maxwell equations (17.10) and (17.11) are

$$\partial_\mu F^{\mu\nu} = \tilde{\theta}\delta\left(F_\Sigma(\mathbf{x})\right) n_\mu \tilde{F}^{\mu\nu} + 4\pi j^\nu. \tag{17.14}$$

In the Lorenz gauge $\partial_\mu A^\mu = 0$, the 4-potential satisfies the equation of motion

$$\left[\eta^\mu{}_\nu \partial^2 - \tilde{\theta}\delta\left(F_\Sigma(\mathbf{x})\right) n_\rho \epsilon^{\rho\mu\alpha}{}_\nu \partial_\alpha\right] A^\nu = 4\pi j^\mu, \qquad \partial^2 = \partial_t^2 - \nabla^2 \tag{17.15}$$

together with the boundary conditions

$$\Delta A^\mu\big|_\Sigma = 0, \qquad \Delta\left(\partial_z A^\mu\right)\big|_\Sigma = -\tilde{\theta}\epsilon^{3\mu\alpha}{}_\nu \left(\partial_\alpha A^\nu\right)\big|_\Sigma, \tag{17.16}$$

which reproduce those written in (17.12)–(17.13) for the electric and magnetic fields.

To obtain a general solution for the potential A^μ in the presence of arbitrary external sources $j^\mu(x)$, we introduce the GF $G^\nu{}_\sigma\left(x, x'\right)$ solving (17.15) for a point-like source,

$$\left[\eta^\mu{}_\nu \partial^2 - \tilde{\theta}\delta\left(F_\Sigma(\mathbf{x})\right) n_\rho \epsilon^{\rho\mu\alpha}{}_\nu \partial_\alpha\right] G^\nu{}_\sigma\left(x, x'\right) = 4\pi \eta^\mu_\sigma \delta^4\left(x - x'\right), \tag{17.17}$$

together with the boundary conditions derived from (17.16), in such a way that the solution for the 4-potential in the Lorenz gauge is

$$A^\mu(x) = \int d^4x'\, G^\mu{}_\nu\left(x, x'\right) j^\nu\left(x'\right), \tag{17.18}$$

up to homogeneous contributions.

As we will show in the following, a further simplification arises when the system satisfies the following two coordinate conditions:(i) the coordinate system can be chosen so that the interface Σ is defined by setting constant only one of them and (ii) the Laplacian is separable in these coordinates in such a way that a complete orthonormal set of eigenfunctions can be defined in the subspace orthogonal to the coordinate defining the interface. Three cases show up immediately: (i) a planar interface at fixed z, (ii) a spherical interface at constant r and (iii) a cylindrical

interface at constant ρ. In all this cases the characteristic function $\theta(\mathbf{x})$ defined in (17.9) can be written in terms of the Heaviside function H of one coordinate like $H(z-a)$, $H(r-a)$ and $H(\rho-a)$, respectively, with the associated unit vectors $\hat{\mathbf{n}}$ given by $\hat{\mathbf{k}}$, $\hat{\mathbf{r}}$ and $\hat{\boldsymbol{\rho}}$, in each of the adapted coordinate systems. Then (17.17) reduces to

$$\left[\eta^{\mu}{}_{\nu}\partial^2 - \tilde{\theta}\delta(\xi-\xi_0)\,\epsilon^{\xi\mu\alpha}{}_{\nu}\partial_\alpha\right] G^{\nu}{}_{\sigma}(x,x') = 4\pi\,\eta^{\mu}{}_{\sigma}\delta^4(x-x'), \tag{17.19}$$

where ξ denotes the coordinate defining the interface at $\xi=\xi_0$ and the coupling of the θ-term is given by a one dimensional delta function with support only at ξ_0. Also, the unit vector $\hat{\mathbf{n}}$ will have a component only in the direction ξ.

Let us illustrate the procedure sketched above by taking the static case of a planar interface located at $z=a$, separating two semi-infinite TIs, such that the MEP is $\theta(z)=\theta_1 H(a-z)+\theta_2 H(z-a)$. In the Coulomb gauge the GF $G^{\nu}{}_{\sigma}(\mathbf{x},\mathbf{x}')$ satisfies

$$\left[-\eta^{\mu}{}_{\nu}\nabla^2 - \tilde{\theta}\delta(z-a))\,\epsilon^{3\mu\alpha}{}_{\nu}\partial_\alpha\right] G^{\nu}{}_{\sigma}(\mathbf{x},\mathbf{x}') = 4\pi\,\eta^{\mu}_{\sigma}\delta^3(\mathbf{x}-\mathbf{x}'), \tag{17.20}$$

together with the boundary conditions (17.16). The coordinates are separated according to $\xi=z$, $\xi_0=a$, plus the two remaining x and y defining the plane parallel to the interface (i.e., perpendicular to the z-axis). The separation of the Laplacian is direct

$$\nabla^2 = \frac{\partial^2}{\partial z^2} + \nabla^2_{\parallel}, \qquad \nabla^2_{\parallel} = \frac{\partial^2}{\partial x^2} + \frac{\partial^2}{\partial y^2}, \tag{17.21}$$

with the operator $\nabla^2_{\parallel}$ having the eigenfunctions

$$\Psi_{\mathbf{p}_\parallel}(x,y) = \frac{1}{2\pi} e^{i\mathbf{p}_\parallel\cdot\mathbf{x}_\parallel}\,, \tag{17.22}$$

labelled by the momentum $\mathbf{p}_\parallel=(p_x,p_y)$ parallel to Σ and where $\mathbf{x}_\parallel=(x,y)$. Let us emphasize that the subindex $\parallel$ denotes objects living in the $x-y$ plane, parallel to the interface $z=a$. The eigenfunctions $\Psi_{\mathbf{p}_\parallel}(x,y)$ are a complete and orthonormal set in the $x-y$ plane, satisfying [41]

$$\int dx dy\; \Psi^*_{\mathbf{p}_\parallel}(x,y)\Psi_{\mathbf{p}'_\parallel}(x,y) = \delta^2_{\mathbf{p}_\parallel,\mathbf{p}'_\parallel}, \qquad \int d^2\mathbf{p}_\parallel\, \Psi_{\mathbf{p}_\parallel}(x,y)\Psi^*_{\mathbf{p}_\parallel}(x,y) = \delta^2(\mathbf{x}_\parallel-\mathbf{x}'_\parallel). \tag{17.23}$$

We recall that in the full 3D-space we have $d^3\mathbf{x} = d\mathbf{x}_\parallel\, dz$ and $\delta^3(\mathbf{x}-\mathbf{x}') = \delta^2(\mathbf{x}_\parallel-\mathbf{x}'_\parallel)\delta(z-z')$. Invariance under translation in the $x-y$ plane together with the the properties in (17.23) allow us to simplify (17.20) introducing the reduced GF $g^{\mu}{}_{\nu}(z,z',\mathbf{p}_\parallel)$, such that

$$G^{\mu}{}_{\nu}(\mathbf{x},\mathbf{x}') = 4\pi\int \frac{d^2\mathbf{p}_\parallel}{(2\pi)^2} e^{i\mathbf{p}_\parallel\cdot(\mathbf{x}-\mathbf{x}')_\parallel} g^{\mu}{}_{\nu}(z,z',\mathbf{p}_\parallel)\,. \tag{17.24}$$

For future use we denote $p^\alpha = (0, p_x, p_y, 0) = (0, \mathbf{p}_\parallel)$. Thus, the final representation of the GF in (17.20) is given in terms of the Fourier transform of the reduced GF in the directions x, y parallel to the plane Σ [43]. Due to the antisymmetry of the Levi-Civita symbol, the partial derivative that appears in the second term of (17.20) for the GF does not introduce derivatives with respect to z, but only in the parallel directions. This allows us to write the equation of the reduced GF as

$$\left[\eta^\mu{}_\nu \tilde{\nabla}^2 + i\tilde{\theta}\delta\left(z-a\right)\epsilon^{3\mu\alpha}{}_\nu p_\alpha\right] g^\nu{}_\sigma\left(z, z', \mathbf{p}_\parallel,\right) = \eta^\mu{}_\sigma \delta\left(z-z'\right), \tag{17.25}$$

with $\tilde{\nabla}^2 = \mathbf{p}_\parallel^2 - \partial_z^2$, $\quad p^\alpha p_\alpha = -\mathbf{p}_\parallel{}^2$ and $|\mathbf{p}_\parallel| = p$. In this way we transform the calculation of the reduced GF into a one-dimensional problem with a delta interaction. Moreover, equation (17.25) can be integrated with the knowledge of an additional reduced GF $\mathfrak{g}^\mu{}_\sigma\left(z, z', \mathbf{p}_\parallel\right) = \eta^\mu{}_\sigma \mathfrak{g}(z, z', \mathbf{p}_\parallel)$, satisfying

$$\left(\mathbf{p}_\parallel^2 - \frac{\partial^2}{\partial z^2}\right)\mathfrak{g}(z, z', \mathbf{p}_\parallel) = \delta\left(z-z'\right), \tag{17.26}$$

together with the required boundary conditions. This auxiliary GF results from the limit $\tilde{\theta} = 0$ in (17.25) and we call it the free reduced GF of the problem, emphasizing that arises when the θ-media are absent. These GFs can be taken directly from the vast literature on electrodynamics and constitute the basis for finding the electromagnetic response of a system with the same symmetries, but now in the presence of a θ-medium whose interface defines the corresponding coordinate system. In the planar case of interest and with the usual BCs at infinity, the option is to take [42]

$$\mathfrak{g}(z, z') = \frac{1}{2p} e^{-p|z-z'|}. \tag{17.27}$$

As a first step in the solution of the (17.25) we obtain the integral equation

$$g^\mu{}_\sigma\left(z, z'\right) = \eta^\mu{}_\sigma \mathfrak{g}\left(z, z'\right) - i\tilde{\theta}\epsilon^{3\mu\alpha}{}_\nu p_\alpha \int dz'' \mathfrak{g}\left(z, z''\right)\delta(z''-a) g^\nu{}_\sigma\left(z'', z'\right), \tag{17.28}$$

where the integration over z'' can be readily performed, reducing the problem to a set of coupled algebraic equations. The solution to (17.28) is obtained as the result of the following steps. First we split the index μ into $\mu = 0$ and $\mu = j = 1, 2, 3$ obtaining

$$g^0{}_\sigma\left(z, z'\right) = \eta^0{}_\sigma \mathfrak{g}\left(z, z'\right) - i\tilde{\theta}\epsilon^{30i}{}_j p_i \mathfrak{g}\left(z, a\right) g^j{}_\sigma\left(a, z'\right), \tag{17.29}$$

$$g^j{}_\sigma\left(z, z'\right) = \eta^j{}_\sigma \mathfrak{g}\left(z, z'\right) - i\tilde{\theta}\epsilon^{3ji}{}_0 p_i \mathfrak{g}\left(z, a\right) g^0{}_\sigma\left(a, z'\right). \tag{17.30}$$

Next we evaluate (17.30) at $z = a$ and substitute $g^j{}_\sigma\left(a, z'\right)$ in (17.29), yielding

$$g^0{}_\sigma\left(z,z'\right)=\eta^0{}_\sigma\mathfrak{g}\left(z,z'\right)-i\tilde{\theta}\epsilon^{30i}{}_j p_i\eta^j{}_\sigma\mathfrak{g}\left(z,a\right)\mathfrak{g}\left(a,z'\right)-\tilde{\theta}^2p^2\mathfrak{g}\left(z,a\right)\mathfrak{g}\left(a,a\right)g^0{}_\sigma\left(a,z'\right). \tag{17.31}$$

Setting $z=a$ in the above equation, we solve for $g^0{}_\sigma\left(a,z'\right)$ which we substitute back to obtain $g^0{}_\sigma\left(z,z'\right)$ in terms of the free GF $\mathfrak{g}\left(z,z'\right)$. The remaining components are obtained after substituting $g^0{}_\sigma\left(a,z'\right)$ in (17.30). The final result is

$$g^\mu{}_\nu\left(z,z'\right)=\eta^\mu{}_\nu\mathfrak{g}\left(z,z'\right)+A\left(z,z'\right)\left\{\tilde{\theta}\mathfrak{g}\left(a,a\right)\left[p^\mu p_\nu+\left(\eta^\mu{}_\nu+n^\mu n_\nu\right)p^2\right]+i\epsilon^\mu{}_\nu{}^{\alpha 3}p_\alpha\right\}, \tag{17.32}$$

where $n_\mu=(0,0,0,1)$ and

$$A\left(z,z'\right)=-\tilde{\theta}\frac{\mathfrak{g}\left(z,a\right)\mathfrak{g}\left(a,z'\right)}{1+p^2\tilde{\theta}^2\mathfrak{g}^2\left(a,a\right)}. \tag{17.33}$$

Extending the above results to the case where one of the media has arbitrary ε, keeping still nonmagnetic materials, we obtain a new version of the (17.32). Going back to the coordinate representation by calculating the Fourier transform in (17.24) we obtain

$$G^0{}_0(\mathbf{x},\mathbf{x}')=\frac{1}{\varepsilon(z')}\left[\frac{1}{|\mathbf{x}-\mathbf{x}'|}-\frac{\mathrm{sgn}(z')\,2(\varepsilon-1)+\tilde{\theta}^2}{2(\varepsilon+1)+\tilde{\theta}^2}\frac{1}{\sqrt{R^2+Z^2}}\right], \tag{17.34}$$

$$G^i{}_0(\mathbf{x},\mathbf{x}')=G^0{}_i(\mathbf{x},\mathbf{x}')=-\frac{2\tilde{\theta}}{2(\varepsilon+1)+\tilde{\theta}^2}\frac{\epsilon^{0ij3}R_j}{R^2}\left(1-\frac{Z}{\sqrt{R^2+Z^2}}\right), \tag{17.35}$$

$$G^i{}_j(\mathbf{x},\mathbf{x}')=\frac{\eta^i{}_j}{|\mathbf{x}-\mathbf{x}'|}-\frac{\tilde{\theta}^2}{2(\varepsilon+1)+\tilde{\theta}^2}\frac{\Lambda^i{}_j}{\sqrt{R^2+Z^2}}+\frac{\tilde{\theta}^2}{2(\varepsilon+1)+\tilde{\theta}^2}\Lambda^r{}_j\partial_r K^i(\mathbf{x},\mathbf{x}'). \tag{17.36}$$

where $Z=|z-a|+|z'-a|$, $\mathbf{R}=(x-x',y-y')$, $R=|\mathbf{R}|$, $\Lambda^i{}_j=\eta^i{}_j+n^in_j$, and

$$K^i\left(\mathbf{x},\mathbf{x}'\right)=\frac{\sqrt{R^2+Z^2}-Z}{R^2}R^i. \tag{17.37}$$

We observe that the substitution of the free reduced GF (17.27) in the expression (17.33) yields that the θ-dependent contribution to the full reduced GF is a function of Z, instead of $|z-z'|$ as it is in the $\tilde{\theta}=0$ contribution. This property is clearly manifest in the expressions written above for the GF components in coordinate space and will have interesting consequences in the case of radiation to be discussed in Sect. 17.5.

The details of the calculations already summarized are presented in [43, 44]. The results for the static GF with spherical and cylindrical symmetries have been extended to the case of ponderable magnetoelectric media with piecewise constant ε and μ in [45, 46]. The MEE has also been explored in the static case by locating a conducting sphere at constant potential in front of a planar TI [47]. Again, we mention that the extension of the above to the case of anisotropic optical properties is possible, and

so is the case for anisotropic MEP. Concretely, the antiferromagnet Cr_2O_3 possess a $\theta_{ij} \sim 1.26 \times 10^{-3}$ (in non-rationalized CGS units), which is however small compared to non magnetoelectric effects. Larger MEE signals can be found in the $TbPO_4$, whose coupling is ~ 0.22 (in non-rationalized CGS units) and the search for giant ME couplings continues mainly in composite multiferroics [48]. An early review of numerous works on the study of infinite linear homogeneous bianisotropic media can be found in [49], which deals mainly with the calculation of the Green functions and the plane-wave propagation in various classes of these media. An alternative way of taking into account magnetoelectric effects in such media would be to introduce interfaces among them. This certainly requires an extension of the methods previously developed. Our GF approach precisely facilitates such extension and this has been one of our motivations.

17.4 The Casimir Effect

The Casimir effect (CE) is one of the most remarkable consequences predicted by quantum field theory as a result of the nonzero energy of the vacuum [50] and has already been experimentally confirmed [51]. For a review of the subject see [52, 53]. Experimental access to probe distances of the order of microns, together with the recent discovery of three-dimensional topological insulators provide additional ground to study the CE [54].

The CE we consider is produced between two perfectly conducting flat surfaces (plates) in vacuum, denoted by P_1 and P_2 and separated by a distance L. Inside this device is placed a planar TI rigidly attached to the surface P_2, as shown in Fig. 17.2. The Σ interface of the TI, located at $z = a < L$, is covered by a very thin magnetized layer. In order to explore the purely topological contribution of the MEP ($\tilde{\theta} \neq 0$) we

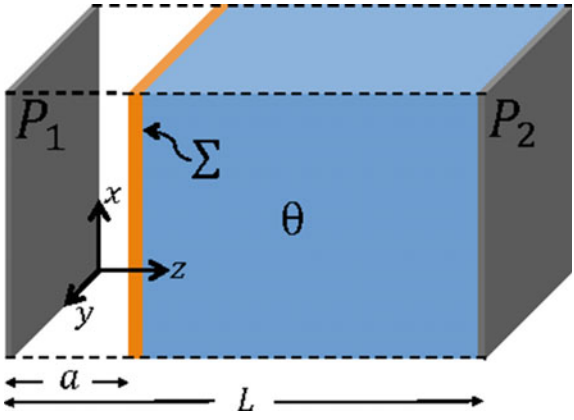

Fig. 17.2 Schematic of the Casimir effect in θ-ED, (adapted from [57])

take both media with $\varepsilon = \mu = 1$, however, non trivial optical properties as well as anisotropy effects can also be considered.

We follow a method similar to that of [42, 55] that begins with the calculation of the corresponding GF, from which the renormalized energy-momentum tensor in the region between the plates is obtained. A subsequent calculation yields the Casimir stress in the interface Σ of the TI. We also consider the limit when the plate P_2 goes back to infinity ($L \to \infty$) to obtain the Casimir stress produced by a single conducting plate in front of a semi-infinite TI. The boundary conditions on the plates P_1 and P_2 are the usual ones for a perfect conductor: $n_\mu \tilde{F}^{\mu\nu}|_{P_{1,2}} = 0$, where $n = (0, 0, 0, 1)$.

This calculation highlights two extensions of our method: (i) the inclusion of time-dependence and (ii) the use of a convenient well-known free reduced GF to obtain the full result. In the absence of free sources at the interface, the GF

$$G^{\mu}{}_{\nu}\left(x, x'\right) = 4\pi \int \frac{d^2\mathbf{p}_\parallel}{(2\pi)^2} e^{i\mathbf{p}_\parallel \cdot \mathbf{x}_\parallel} \int \frac{d\omega}{2\pi} e^{-i\omega(t-t')} g^{\mu}{}_{\nu}\left(z, z'\right), \tag{17.38}$$

satisfies the (17.19), together with the BC of (17.16). From here on we do not write the dependence of the reduced GF $g^{\mu}{}_{\nu}$ on ω and $\mathbf{p}_\parallel$. In the Lorenz gauge, the equation for $g^{\mu}{}_{\nu}$ is

$$\left[\eta^{\mu}{}_{\nu}\partial^2 + i\tilde{\theta}\delta\left(z-a\right)\epsilon^{3\mu\alpha}{}_{\nu}p_\alpha\right] g^{\nu}{}_{\sigma}\left(z, z'\right) = \eta^{\mu}{}_{\sigma}\delta\left(z - z'\right), \tag{17.39}$$

where now we have $\partial^2 = {\mathbf{p}_\parallel}^2 - \omega^2 - \partial_z^2$ and $p^\alpha = \left(\omega, \mathbf{p}_\parallel, 0\right)$.

The boundary contribution in $z = L$, which is not present in (17.39), is identically zero in the distributional sense due to the BCs on the conducting plate P_2. The next step, which illustrates the flexibility of the method developed in the Sect. 17.3, is to choose a free GF to integrate (17.39). It is clear that we must use the free reduced GF corresponding to two perfectly conducting parallel plates located at $z = 0$ and $z = L$, which is given by [42]

$$\mathfrak{g}_C\left(z, z'\right) = \frac{\sin\left[pz_<\right]\sin\left[p\left(L - z_>\right)\right]}{p\sin\left[pL\right]}, \tag{17.40}$$

where the suffix C is for Casimir, $z_>$ ($z_<$) is the greater (smaller) value between the coordinates z, z', and $p = \sqrt{\omega^2 - \mathbf{p}^2}$. Writting the solution of (17.39) as

$$g^{\mu}{}_{\nu}\left(z, z'\right) = \eta^{\mu}{}_{\nu}\mathfrak{g}_C\left(z, z'\right) + g^{\mu}_{C\nu}\left(z, z'\right). \tag{17.41}$$

we realize that the first term corresponds to the absence of the TI between the plates, while the second term, to be called the reduced θ-GF,

$$g^{\mu}_{C\nu}\left(z,z'\right)=\tilde{\theta}\mathfrak{g}_C\left(a,a\right)\left[p^{\mu}p_{\nu}-\left(\eta^{\mu}{}_{\nu}+n^{\mu}n_{\nu}\right)p^2\right]A_C\left(z,z'\right)+i\,\epsilon^{\mu}{}_{\nu}{}^{\alpha 3}p_{\alpha}A_C\left(z,z'\right),$$
$$A_C\left(z,z'\right)=-\tilde{\theta}\frac{\mathfrak{g}_C\left(z,a\right)\mathfrak{g}_C\left(a,z'\right)}{1-p^2\tilde{\theta}^2\mathfrak{g}_C^2\left(a,a\right)}, \tag{17.42}$$

will be responsible for the effect we are looking for. The partition in (17.41) yields the full GF as $G^{\mu}{}_{\nu}\left(x,x'\right)=\eta^{\mu}{}_{\nu}\mathcal{G}\left(x,x'\right)+G^{\mu}_{C\nu}\left(x,x'\right)$, where each term arises from the respective contribution in (17.41). Since the MEP modifies the behavior of the fields only in the interface, the energy-momentum tensor (EMT) $T^{\mu\nu}$ in the bulk retains the original expression of the unmodified Maxwell equations, failing to be conserved only in the interface in the absence of free external sources [45]. Next we determine the vacuum expectation value (VEV) of $T^{\mu\nu}$, to be called the vacuum stress (VE), according to the basic relation $G^{\mu\nu}(x,x)=-i\langle 0|\mathcal{T}A^{\mu}(x)A^{\nu}(x')|0\rangle$, where $\mathcal{T}$ denotes time ordering. Following the standard point-splitting method we obtain

$$\begin{aligned}\langle T^{\mu\nu}\rangle=\frac{i}{4\pi}\lim_{x\to x'}\Big[&-\partial^{\mu}\partial'^{\nu}G^{\lambda}{}_{\lambda}+\partial^{\mu}\partial'_{\lambda}G^{\lambda\nu}+\partial^{\lambda}\partial'^{\nu}G^{\mu}{}_{\lambda}\\&-\partial'^{\lambda}\partial_{\lambda}G^{\mu\nu}+\frac{1}{2}\eta^{\mu\nu}\left(\partial^{\alpha}\partial'_{\alpha}G^{\lambda}{}_{\lambda}-\partial^{\alpha}\partial'_{\beta}G^{\beta}{}_{\alpha}\right)\Big].\end{aligned} \tag{17.43}$$

Again, we can write $\langle T^{\mu\nu}\rangle=\langle t^{\mu\nu}\rangle+\left\langle T_C^{\mu\nu}\right\rangle$. The first term is the contribution to the VE in the absence of the TI, yielding the well-known result in [55], which is independent of a. After some calculation, the second term $\left\langle T_C^{\mu\nu}\right\rangle$, to be called the θ-vacuum stress (θ-VS), is

$$\left\langle T_C^{\mu\nu}\right\rangle=i\tilde{\theta}\int\frac{d^2\mathbf{p}_{\parallel}}{(2\pi)^2}\int\frac{d\omega}{2\pi}\left(p^{\mu}p^{\nu}+n^{\mu}n^{\nu}p^2\right)\mathfrak{g}_C\left(a,a\right)\lim_{z\to z'}\left(p^2+\partial'_z\partial_z\right)A_C\left(z,z'\right). \tag{17.44}$$

Next we require the renormalized VS: $\langle T^{\mu\nu}\rangle_{\text{ren}}=\langle T^{\mu\nu}\rangle-\langle T_C{}^{\mu\nu}\rangle_{\text{vac}}$, where the first (second) term is the VS in the presence (absence) of conducting plates [55, 56]. We obtain

$$\left\langle T_C^{\mu\nu}\right\rangle_{\text{ren}}=-\frac{\pi^2}{720L^4}\left(\eta^{\mu\nu}+4n^{\mu}n^{\nu}\right)\left[u(\theta,\chi)H\left(a-z\right)+u(\theta,1-\chi)H\left(z-a\right)\right], \tag{17.45}$$
$$u(\theta,\chi)=\frac{120}{\pi^4}\int_0^{\infty}\frac{\tilde{\theta}^2\xi^3\,\mathrm{sh}\left[\xi\chi\right]\mathrm{sh}^3\left[\xi\left(1-\chi\right)\right]\mathrm{sh}^{-3}\left[\xi\right]}{1+\tilde{\theta}^2\mathrm{sh}^2\left[\xi\chi\right]\mathrm{sh}^2\left[\xi\left(1-\chi\right)\right]\mathrm{sh}^{-2}\left[\xi\right]}d\xi. \tag{17.46}$$

The notation is $\mathrm{sh}(x)=\sinh(x)$ and $\chi=a/L$ with $0<\chi<1$. Our expression (17.45) has the same tensorial structure as that in [55], except for a z dependence because the EMT is not conserved at the interface, implying that the renormalized θ-VS is constant in each bulk but has a discontinuity in $z=a$ consistent with $\partial_z\left\langle T_C^{00}\right\rangle_{\text{ren}}\propto\delta(\Sigma)$.

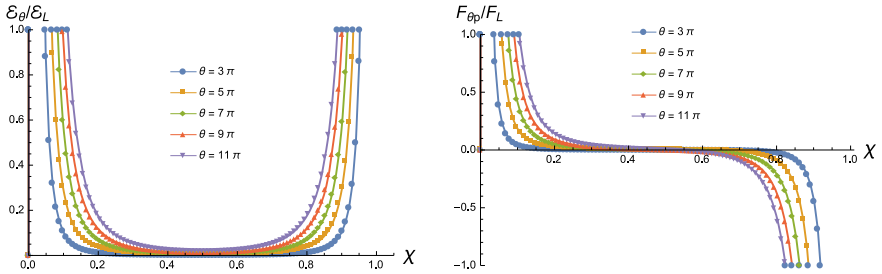

Fig. 17.3 Left panel: the ratio $\mathcal{E}_\theta/\mathcal{E}_L$. Right panel: the Casimir pressure at the interface in units of F_L. Both plots are in terms of the the dimensional parameter $\chi = a/L$ and for different values of θ, (adapted from [57])

The Casimir energy $\mathcal{E} = \mathcal{E}_L + \mathcal{E}_\theta$ is defined as the energy per unit area stored by the electromagnetic field in the region between the conducting plates. Let us recall that $\mathcal{E}_L = -\pi^2/(720L^3)$ is the Casimir energy in the absence of the TI. The relevant contribution is

$$\mathcal{E}_\theta = \int_0^L dz \left\langle T_C^{00} \right\rangle_{\text{ren}} = \mathcal{E}_L \left[\chi u(\theta, \chi) + (1-\chi)u(\theta, 1-\chi)\right]. \tag{17.47}$$

The first term is the energy stored between the plate P_1 and the interface, while the second term corresponds to the energy stored in the bulk of the TI. The Casimir pressure $F_{\theta p}$ on the interface is $F_{\theta p} = -d\mathcal{E}_\theta/da$, yielding

$$\frac{F_{\theta p}}{F_L} = -\frac{1}{3}\frac{d}{d\chi}\left[\chi u(\theta, \chi) + (1-\chi)u(\theta, 1-\chi)\right], \qquad F_L = -\pi^2/(240L^4). \tag{17.48}$$

The ratios $\mathcal{E}_\theta/\mathcal{E}_L$ (left panel) and $F_{\theta p}/F_L$ (right panel) as a function of χ, for different values of θ are plotted in Fig. 17.3 [57]. Our setup is a 3D analogue of the Casimir piston [58], and we obtain the similar result that the Casimir pressure tends to pull the interface towards the closest conducting plate, as shown in the right panel of the Fig. 17.3. When the plate P_2 recedes to infinity, $L \to \infty$, our setup describes the Casimir interaction between a perfect conducting plate P_1 at a distance a from a semi infinite TI. The Casimir energy (17.47) is now $\mathcal{E}_\theta^{L\to\infty} = \mathcal{E}_a R(\theta)$, with $\mathcal{E}_a = -\pi^2/720a^3$. The function

$$R(\theta) = \frac{120}{\pi^4}\int_0^\infty \xi^3 \frac{\tilde{\theta}^2}{1+\tilde{\theta}^2 e^{-2\xi}\sinh^2\xi} e^{-3\xi}\sinh\xi\, d\xi, \tag{17.49}$$

turns out to be independent of a and it is bounded by its limit $\theta \to \pm\infty$. In this way

Table 17.1 The normalized pressure $f_\theta = F_\theta^{L\to\infty}/F_a = R(\theta)$ for different values of θ

θ	$\pm 7\pi$	$\pm 15\pi$	$\pm 23\pi$	$\pm 31\pi$	$\pm 39\pi$
f_θ	0.0005	0.0025	0.0060	0.0109	0.0172

$$R(\theta) \leq \frac{120}{\pi^4}\int_0^\infty \xi^3 \frac{e^{-\xi}}{\sinh\xi} d\xi = 1. \tag{17.50}$$

Physically, this means that in the limit $\theta \to \infty$, the interface Σ behaves as a conducting plate. This is analogous to the Schwinger prescription that a perfect conductor is obtained in the limit $\varepsilon \to \infty$ of a dielectric material [42]. In the limit $L \to \infty$ the Casimir pressure is $f_\theta = F_\theta^{L\to\infty}/F_a = R(\theta)$, with $F_a = -\pi^2/240a^4$. In Table 17.1 we show some numerical results for f_θ for different values of θ.

The θ dependence of the Casimir pressure could be used to determine the corresponding MEP. This pressure has been measured for separation distances L between the metal plates in the range of 0.5–3.0 μm [51], which will require to prepare TIs with widths smaller than these amounts. In addition, the ratios for f_θ indicated in Table 17.1 allow us to estimate that an increase of several orders of magnitude would be required in the experimental accuracy. The particular values of $\theta = \pm 7\pi, \pm 15\pi$ are suitable for a TI such as $Bi_{1-x}Se_x$ [59]. The CE could be explored in TIs with higher values of $\tilde{\theta} = (2n+1)\pi$, however these material features magnetoelectric couplings that are not considered in our model based on θ-ED [60, 61].

As discussed above, the nondynamical axion electrodynamics can be seen as a particular realization of the photon sector of the Standard Model Extension with the identification $(k_F)_{\kappa\lambda\mu\nu} = \theta(x)\epsilon_{\kappa\lambda\mu\nu}$. The Casimir effect has also been analyzed within the context of the SME, for arbitrary $(k_F)_{\kappa\lambda\mu\nu}$ and $(k_{AF})^\kappa$ Lorentz-violating couplings [62, 63].

17.5 Reversed Vavilov-Cherenkov (VC) Radiation in Naturally Existing Magnetoelectric Media

In this section we summarize the discovery reported in the [64] of reversed VC radiation (RVCR) in naturally occurring magnetoelectric materials. The usual VC radiation is produced when a charge q propagates with velocity $v > c/n$ in a medium with refraction index n, i. e., with a velocity higher than the speed of light in the material [65, 66]. The first theoretical description of such radiation in the framework of Maxwell's theory, developed by Frank and Tamm in [67], revealed its unique polarization and directional properties. In particular, VC radiation is localized in a forward cone with opening angle $\alpha = \arccos(vn/c)$. VC radiation has played a fundamental

role in the study of high-energy particle physics, high-power microwave sources and nuclear and cosmic-ray physics [68, 69], both theoretically and experimentally.

In 1968 Veselago theoretically proposed that RVCR could be produced in materials having simultaneously a negative permittivity and permeability, dubbed as left-handed media (LHM). A medium is left-handed when the momentum $\mathbf{k}$ of a propagating electromagnetic wave is antiparallel to its Poynting vector $\mathbf{E} \times \mathbf{B}$, i. e., when the group velocity and the phase velocity of the wave are antiparallel [70]. In this case photons would be emitted in the backward direction with respect to the velocity of the propagating charge. Since these materials are not found in nature, this proposal has generated a great boost to the design and construction of metamaterials, that is, artifacts built in the laboratory that can reproduce these properties in certain frequency ranges. In recent years the study of RVCR has been of considerable interest [71–79]. The realization of a LHM in an interface between an ordinary media was experimentally proved in [80]. It is interesting that Reversed Cherenkov radiation has also been found for sound in topological insulators in [81, 82].

Let us consider two semi infinite magnetoelectric media ($\theta_1 \neq \theta_2$) separated by a planar interface Σ located at $z = 0$. The setup is described by θ-ED according to the conventions in Sect. 17.2 and the modified Maxwell equations are (17.4). This time we take into account the permittivity of the media, but choose $\epsilon_1 = \epsilon_2 = \epsilon$ to avoid the interference with transition radiation. Still we consider non-magnetic media with $\mu_1 = \mu_2 = 1$. These choices provide a first approximation to the problem which aims to single out the effects of the axion coupling, determined by $\tilde{\theta} = \alpha(\theta_2 - \theta_1)/\pi$.

The electric and magnetic fields are obtained from (17.6) after the potential A_μ is expressed in terms of the GF according to (17.18). The GF $G^\nu{}_\sigma(x, x')$ satisfies the equation

$$\left(\left[\Box^2\right]^\mu{}_\nu - \tilde{\theta}\delta(z)\varepsilon^{3\mu\alpha}{}_\nu\partial_\alpha\right) G^\nu{}_\sigma(\mathbf{x}, \mathbf{x}', t - t') = 4\pi\eta^\mu{}_\sigma\delta^4(x - x') \tag{17.51}$$

and its calculation is analogous to the static case in Sect. 17.3. The main differences with respect to (17.20) arise in the inclusion of the time dependence together with setting $\epsilon \neq 1$ and they are reflected in the changes $-\eta^\mu_\nu\nabla^2 \to \left[\Box^2\right]^\mu{}_\nu = \left(\epsilon\Box^2, \Box^2\delta^i{}_j\right)$ with $\Box^2 = \epsilon\partial_t^2 - \nabla^2$. An additional Fourier transform involving $\exp i\omega(t - t')$ in (17.24) allows to write the GF in terms of the reduced GF $g^\nu{}_\sigma(z, z', \mathbf{p}_\parallel, \omega)$ which satisfies an equation similar to (17.25). In this case, the free reduced GF, $\mathcal{F}_0(z, z'; \mathbf{k}_\parallel, \omega)$, satisfies $\left(\mathbf{p}_\parallel^2 - \omega^2\epsilon - \partial_z^2\right)\mathcal{F}_0(z, z'; \mathbf{k}_\parallel, \omega) = \delta(z - z')$, plus the standard BCs at infinity. The result is [87]

$$\mathcal{F}_0(z, z'; \mathbf{p}_\parallel, \omega) = \frac{ie^{ik_z|z-z'|}}{2k_z}, \qquad k_z = \sqrt{\epsilon\omega^2 - \mathbf{p}_\parallel^2}. \tag{17.52}$$

The solution of the subsequent coupled algebraic equations yields a result for $g^\nu{}_\sigma(z, z', \mathbf{p}_\parallel, \omega)$ in terms of $\mathcal{F}_0(z, z'; \mathbf{p}_\parallel, \omega)$ whose θ-dependent contribution shows a dependence on $|z| + |z'|$, as it was the case in the static situation. The knowledge of the reduced GF yields the coordinate representation $G^\nu{}_\sigma(\mathbf{x}, \mathbf{x}', \omega)$ in terms

of a Fourier transform in the parallel momentum space, as indicated in (17.24), whose components are explicitly given in (43) of [64]. The next step is to evaluate the GF in the far-field approximation corresponding to the coordinate conditions $r \equiv \|\mathbf{x}\| \gg \|\mathbf{x}'\|$, $R_\parallel \equiv \| \left(\mathbf{x} - \mathbf{x}'\right)_\parallel \| \simeq \|\mathbf{x}_\parallel\|$, $|z| + |z'| \simeq |z|$. In this approximation the required integrals yielding the Fourier transforms include rapidly oscillating exponential functions whose leading contributions are calculated in the steepest descent method [83–85]. Also we make repeated use of the generic Sommerfeld identity [86]

$$i \int_0^\infty \frac{k_\parallel dk_\parallel}{\sqrt{\tilde{k}_0^2 - k_\parallel^2}} J_0(k_\parallel R_\parallel) e^{i\sqrt{\tilde{k}_0^2 - k_\parallel^2}|Z|} = \frac{e^{i\tilde{k}_0 \mathcal{R}}}{\mathcal{R}}, \qquad \tilde{k}_0 = \sqrt{\epsilon}\omega, \tag{17.53}$$

with $\mathcal{R} = \sqrt{R_\parallel^2 + Z^2}$ and $n = \sqrt{\epsilon}$ being the refraction index. Two cases appear: (i) $Z = |z - z'|$, where $\mathcal{R}$ is denoted by R, corresponding to the usual $\tilde{\theta} = 0$ contribution and (ii) $Z = |z| + |z'|$, where $\mathcal{R}$ is denoted by $\bar{R}$ and which involves the effects of the axion coupling. It is pertinent to emphasize an important difference in the phase of the exponentials related to the source variables $\mathbf{x}'$ in these two different cases. In the choice (i) we encounter the exponential $e^{i\tilde{k}_0 R}$, which in the coordinate approximation of the far-field zone produces the phase $i\tilde{k}_0(r - \hat{\mathbf{x}} \cdot \mathbf{x}'_\parallel - z' \cos\theta) = i\tilde{k}_0(r - \hat{\mathbf{x}} \cdot \mathbf{x}')$ characteristic of radiation in standard electrodynamics [87]. Here $\hat{\mathbf{x}} = \mathbf{x}/\|\mathbf{x}\|$. On the other hand, the contributions to the GF involving the axion coupling arising from the choice (ii) include the exponential $e^{i\tilde{k}_0 \bar{R}}$ with

$$\begin{aligned} \tilde{R} &= \sqrt{(\mathbf{x} - \mathbf{x}')_\parallel^2 + (|z| + |z'|)^2} = \sqrt{(\mathbf{x} - \mathbf{x}')^2 - (z - z')^2 + (|z| + |z'|)^2} \\ &= \sqrt{(\mathbf{x} - \mathbf{x}')^2 + 2(|zz'| + zz')} \sim r - \hat{\mathbf{x}} \cdot \mathbf{x}'_\parallel + |z' \cos\theta|, \end{aligned} \tag{17.54}$$

in the far-field approximation. From the square root in second line of (17.54) we remark that whenever the sign of $zz' = r\cos\theta z'$ is positive we will have an additional relative phase contributing to the GFs, which will show up in observable quantities as the radiated power for example. The term $(|z| + |z'|)^2$ can ultimately be traced back to the form of the reduced GF, as mentioned before. In the following we will show that RVCR arises precisely due to the contribution $|z' \cos\theta|$ in the phase of the GF. The detailed calculation is presented in the Appendix of [64] and here we only summarize the results emphasizing the phase dependence of the contributions. The full GF $G^\mu{}_\nu$ can be written in terms of the auxiliary function $\bar{G}^\mu{}_\nu = \bar{G}^\mu{}_{ED\,\nu} + \bar{G}^\mu{}_{\tilde{\theta}\,\nu} + \bar{G}^\mu{}_{\tilde{\theta}^2\,\nu}$ such that $G^0{}_0 = \bar{G}^0{}_0/\epsilon$ and $G^\mu{}_\nu = \bar{G}^\mu{}_\nu$ for the remaining cases. In the far field approximation we find

$$\bar{G}^{\mu}_{ED\ \nu}(\mathbf{x},\mathbf{x}';\omega) = \eta^{\mu}_{\ \nu}\frac{e^{i\tilde{k}_0 r}}{r}e^{-i\tilde{k}_0\,\hat{\mathbf{x}}\cdot\mathbf{x}'},$$

$$\bar{G}^{\mu}_{\tilde{\theta}\ \nu}(\mathbf{x},\mathbf{x}';\omega) = \varepsilon^{\mu}_{\ \nu\ \alpha 3}\frac{2\tilde{\theta}}{4n^2+\tilde{\theta}^2}\frac{s_\alpha}{|\cos\theta|}\frac{e^{i\tilde{k}_0 r}}{r}e^{i\tilde{k}_0\left(-\hat{\mathbf{x}}\cdot\mathbf{x}'_{\parallel}+|z'\cos\theta|\right)},$$

$$\bar{G}^{\mu}_{\tilde{\theta}^2\ \nu}(\mathbf{x},\mathbf{x}';\omega) = \frac{\tilde{\theta}^2}{4n^2+\tilde{\theta}^2}\frac{e^{i\tilde{k}_0 r}}{r\cos^2\theta}C^{\mu}_{\ \nu}(\theta,\phi,n)\times e^{i\tilde{k}_0\left(-\hat{\mathbf{x}}\cdot\mathbf{x}'_{\parallel}+|z'\cos\theta|\right)}, \quad (17.55)$$

Here $s_\alpha = (1/n, \hat{\mathbf{x}})$ and θ, ϕ are the standard spherical angles labelling the unit vector $\hat{\mathbf{x}}$.

Now we choose our source by considering a point charge q moving with a constant velocity $v\hat{\mathbf{u}}$ in direction perpendicular to the interface Σ which is described by the charge and current densities $\varrho(\mathbf{x}';\omega) = \frac{q}{v}\delta(x')\delta(y')e^{i\omega\frac{z'}{v}}$ and $\mathbf{j}(\mathbf{x}';\omega) = \varrho v\hat{\mathbf{u}}$, respectively. Here $\hat{\mathbf{u}}$ is the unit vector perpendicular to the the interface and directed from the region $z<0$ to the region $z>0$. In the following we assume $v>0$ and consider the motion in the interval $z\in(-\zeta,\zeta)$, with $\zeta \gg v/\omega$, to then take the limit $\zeta\to\infty$. After a long calculation in the far field approximation, we get the electric field starting from the potential A_μ obtained from the convolution of the given source with the GF resulting from (17.55). In this way we are in position to determine the spectral distribution (SD) of the radiation given by

$$d^2E/d\omega d\Omega = (\mathbf{E}^*\cdot\mathbf{E})\,nr^2/4\pi^2 \quad (17.56)$$

in the limit $r\to\infty$. The main point to stress is that the resulting $\mathbf{E}$ turns out to be linear in the following integrals

$$\mathcal{I}_1(\omega,\theta) = \int_{-\zeta}^{\zeta} dz' e^{i\frac{\omega z'}{v}(1-vn\cos\theta)} = \frac{2\sin(\zeta\,\Xi_-)}{\Xi_-}, \quad (17.57)$$

$$\mathcal{I}_2(\omega,\theta) = \int_{-\zeta}^{\zeta} dz' e^{in\omega|z'\cos\theta|+i\omega\frac{z'}{v}} = \frac{\sin(\zeta\,\tilde{\Xi}_-)}{\tilde{\Xi}_-}+\frac{\sin(\zeta\,\tilde{\Xi}_+)}{\tilde{\Xi}_+}+2i\frac{\sin^2(\frac{\zeta}{2}\tilde{\Xi}_-)}{\tilde{\Xi}_-} - 2i\frac{\sin^2(\frac{\zeta}{2}\tilde{\Xi}_+)}{\tilde{\Xi}_+}. \quad (17.58)$$

The notation is $\Xi_- = \frac{\omega}{v}(1-vn\cos\theta)$ and $\tilde{\Xi}_\pm = \frac{\omega}{v}(1\pm vn|\cos\theta|)$. Moreover, in the limit $\zeta\to\infty$, the right hand side in (17.57) and (17.58) yields contributions of the type $\sin(\zeta\ \rho N)/(\rho N)$ which behave like $\pi\delta(\rho N)$. This implies that the non-zero contributions to the electric field arise from those terms whose arguments Ξ_- and $\tilde{\Xi}_\pm$ can take the value zero. With our previous conventions ($vn>0$) this condition eliminates the dependence on $\tilde{\Xi}_+$ as a possible candidate. The remaining possibilities are (i) $1-vn\cos\theta=0$ and/or (ii) $1-vn|\cos\theta|=0$. The first case contributes to the standard VC radiation yielding $\cos\theta_C = 1/(nv)$. Case (ii) opens up the possibility

that $\cos\theta < 0$, yielding a radiation cone with angle $\theta_{\rm R} = \pi - \theta_C$ which signals the reversed VC radiation. In other words, the term containing $\tilde{\Xi}_-$ makes possible the production of radiation in the backward direction with respect to the moving charge. The total SD of the radiation is the sum of the following three contributions

$$\frac{d^2E_1}{d\omega d\Omega} = \frac{n\omega^2 q^2}{\pi^2}\left(1 - \frac{1}{v^2n^2}\right)\frac{\sin^2(\zeta\,\Xi_-)}{\Xi_-^2}, \tag{17.59}$$

$$\frac{d^2E_{12}}{d\omega d\Omega} = -\frac{n\omega^2}{\pi^2}\frac{\tilde{\theta}^2 q^2}{4n^2+\tilde{\theta}^2}\left(1 - \frac{1}{v^2n^2}\right)\frac{\sin(\zeta\,\Xi_-)\sin\left(\zeta\,\tilde{\Xi}_-\right)}{\Xi_-\,\tilde{\Xi}_-}, \tag{17.60}$$

$$\frac{d^2E_2}{d\omega d\Omega} = \frac{n\omega^2}{4\pi^2}\frac{\tilde{\theta}^2 q^2}{4n^2+\tilde{\theta}^2}\left(1 - \frac{1}{v^2n^2}\right)\left[\frac{\sin^2\left(\zeta\,\tilde{\Xi}_-\right)}{\tilde{\Xi}_-^2} + \frac{\sin^4\left(\frac{\zeta}{2}\,\tilde{\Xi}_-\right)}{\frac{1}{4}\tilde{\Xi}_-^2}\right]. \tag{17.61}$$

Equation (17.59) gives the SD of standard VC radiation ($\cos\theta_C = 1/(nv) > 0$), which acquires $\tilde{\theta}$-dependent corrections from the remaining contributions. Let us observe that (17.60) contributes only to the forward radiation. The reversed VC radiation, which is strictly zero for normal insulators, arises only from the term in (17.61) which nevertheless also contributes to the forward output.

The total energy per unit frequency and per unit length radiated by the charge on its path from $-\zeta$ to $+\zeta$ is calculated along the steps in [88] integrating the solid angle and taking into account that the delta-like behavior of the integrands shows that the radiation is sharply localized in a main lobe around the angles θ_C of the forward/backward cone. Such lobes produce the final cones of radiation when $\zeta \to \infty$. The results for the forward and reversed VC radiation are:

$$\frac{d^2E_{\rm FVCR}}{d\omega\, dL} = q^2\omega\left(1 - \frac{1}{v^2n^2}\right)\left[1 - \frac{1}{2}\frac{\tilde{\theta}^2}{4n^2+\tilde{\theta}^2}\right], \tag{17.62}$$

$$\frac{d^2E_{\rm RVCR}}{d\omega\, dL} = q^2\omega\left(1 - \frac{1}{v^2n^2}\right)\left[\frac{1}{2}\frac{\tilde{\theta}^2}{4n^2+\tilde{\theta}^2}\right], \tag{17.63}$$

respectively. We have introduced the total length $L = 2\zeta$ travelled by the particle.

To illustrate our results, we consider medium 2 as the topological insulator $TlBiSe_2$, with $n_2 = 2$, together with a normal insulator as medium 1, characterized by $n_1 = n_2$. We consider the radiation emitted at a frequency of $\omega = 2.5$ eV (500 nm), which constitutes an average in the Cherenkov radiation spectrum. The angular distribution of the total radiation is shown in Fig. 17.4. In the left panel we plot an enlargement of the angular distribution in the backward direction, which shows the appearance of the reversed VC radiation and makes its suppression evident with respect to the forward output, which is given by the ratio $\tilde{\theta}^2/8n^2$ between the results (17.63) and (17.62). A comparison with measurements of reversed VC radiation in metamaterials can be established by interpreting this suppression as due to the detection of radiation at an effective frequency $\omega_{\rm eff} = \omega\,\tilde{\theta}^2/8n^2$. Taking an average of 500 nm (2.5 eV) in the Cherenkov spectrum, we would expect

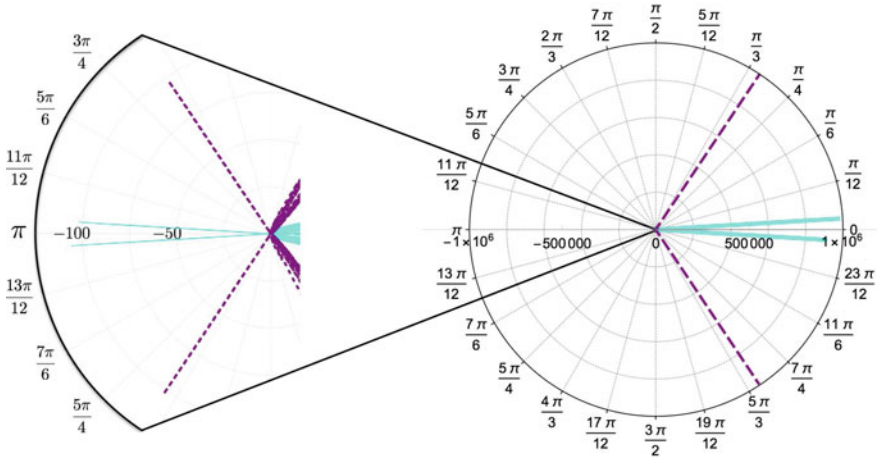

Fig. 17.4 Angular distribution for the total radiated energy per unit frequency for the full VC radiation for the choices for $n = 2$, $\omega = 2.48$ eV and $\tilde{\theta} = 11\alpha$. The dashed purple line corresponds to $v = 0.9$ and $\zeta = 343\,\text{eV}^{-1}$, and the solid cyan line to $v = 0.5009$ and $\zeta = 4830\,\text{eV}^{-1}$. The scale of the polar plot is in arbitrary dimensions and runs from 0 to 10^6. In the left side of the figure we plot an enlargement in the backward direction showing the onset of the reversed VC radiation. Here the radial scale goes from zero to 10^2. The charge moves from left to right, (adapted from [64])

the production of reversed VC radiation at effective frequencies ω_{eff} in the range from 4×10^{-3} meV for $\tilde{\theta} = \alpha$ to 0.5 meV for $\tilde{\theta} = 11\alpha$ respectively, using $TlBiSe_2$ as a θ-medium. Recent measurements of reversed VC radiation in metamaterials show that this estimations are within the experimental capabilities. Reversed VC radiation has been measured at a frequency of 2.85 GHz (1.2×10^{-2} meV), in an all-metal metamaterial consisting of a square waveguide loaded with complementary electric split ring resonators [78]. Likewise, reversed VC radiation in the range $(3.4 - 3.9) \times 10^{-2}$ meV has also been experimentally verified in a phased electromagnetic dipole array used to model a moving charged particle [76]. We have also estimated that $d^2E_{\text{RVCR}}/dtd\omega = vd^2E_{\text{RVCR}}/d\omega\, dL$ is within the range $10^{-3} - 10^{-2}$ μW/eV for the frequency interval $\omega = 2 - 8$ eV. Such values are smaller by a factor of $10^{-4} - 10^{-3}$ than the maximum output of ~ 10 μW/eV theoretically predicted to occur in the narrow interval of $5.7 - 6.5$ eV in a metal-insulator-metal waveguide [79]. In such a waveguide with a core thickness of $a = 20$ nm, surface plasmon polaritons excited by an electron moving at $v = 0.8$ produce reversed VC radiation.

The main features of the RVCR we have found are: (i) the threshold condition $v > 1/n$ must be satisfied as in the usual case, (ii) RVCR occurs for all frequencies

in the Cherenkov spectrum and is always accompanied by forward radiation with the same frequency, (iii) the angular distribution of the RVCR is suppressed with respect to the forward emission by a factor $\tilde{\theta}^2/8n^2$. The details of this development are reported in [64].

17.6 Electromagnetic Response of Weyl Semimetals

In addition to the topological insulators, which are characterized by a gapped bulk and protected boundary modes that are robust against disorder [19–22], we have recently learned that gapless semimetallic states may be topologically nontrivial in the same sense as gapped insulators. Weyl semimetals are topological states of matter in which the 3D bulk contains Weyl points (band crossing points) protected by crystalline symmetries and whose low-energy quasiparticles are linearly dispersing massless Weyl fermions. Weyl semimetals possess protected gapless surface states on disconnected Fermi arcs with end points at the projection of the bulk nodes onto the surface Brillouin zone [24].

Besides their spectroscopic distinguishing features, WSMs also exhibit unusual electromagnetic responses that are a direct macroscopic manifestation of the nontrivial topology of their band structure. Mathematically, the anomalous Hall effect and related effects to the chiral anomaly may be compactly expressed as an induced θ term in the action of the electromagnetic field, when chiral fermions are integrated out [89–91]:

$$S_\theta = \frac{\alpha}{4\pi^2}\int \theta(\mathbf{r},t)\,\mathbf{E}\cdot\mathbf{B}\,dt\,d^3\mathbf{r}, \tag{17.64}$$

where $\alpha = e^2/\hbar c$ is the fine-structure constant and $\theta(\mathbf{r},t)$ is the axion field, with the following form

$$\theta(\mathbf{r},t) = 2\mathbf{b}\cdot\mathbf{r} - 2b_0 t, \tag{17.65}$$

where $2\mathbf{b}$ is the separation, in momentum space, between Weyl nodes and $2b_0$ their separation in energy. Topological response of WSMs is thus described by an action similar to that of axion-electrodynamics [36]. The relevant equations of motion are obtained by varying the full action (S_θ plus the nontopological Maxwell action):

$$\nabla\cdot\mathbf{D} = 4\pi\left(\rho - \frac{\alpha}{2\pi^2}\mathbf{b}\cdot\mathbf{B}\right), \tag{17.66}$$

and

$$\nabla\times\mathbf{H} - \frac{1}{c}\frac{\partial\mathbf{D}}{\partial t} = \frac{4\pi}{c}\left(\mathbf{J} + \frac{\alpha}{2\pi^2}c\mathbf{b}\times\mathbf{E} - \frac{\alpha}{2\pi^2}b_0\mathbf{B}\right), \tag{17.67}$$

where $\mathbf{D} = \varepsilon\,\mathbf{E}$ and $\mathbf{B} = \tilde{\mu}\,\mathbf{H}$. Faraday's law, $\nabla \times \mathbf{E} = -c^{-1}\partial\mathbf{B}/\partial t$, and the equation stating the absence of magnetic monopoles, $\nabla \cdot \mathbf{B} = 0$, remain unaltered. Here, as in ordinary metals, $\varepsilon = \epsilon + i\sigma_{xx}(\omega)/\omega$ and $\tilde{\mu} = 1 + \chi_m$, where ϵ is the static permittivity, $\sigma_{xx}(\omega)$ is the longitudinal conductivity and χ_m is the magnetic susceptibility that we assume is negligible for the WSM. Again, we will treat the WSM material as linear and isotropic, but the extension to the linear and anisotropic case is possible.

There are other distinguishing effects of Weyl semimetals not fully captured by axion electrodynamics, such as the chiral magnetic effect and the chiral separation effect. These can be derived by using, for example, the semiclassical Boltzmann transport theory. In short, if we have chiral fermions in a magnetic field with chemical potentials μ_{L} and μ_{R} for left- and right-handed fermions, respectively, there are two additional **B**-dependent current terms, namely,

$$\mathbf{J}^{(\mathrm{B})} = \frac{\alpha}{2\pi^2}\mu_5\mathbf{B} \quad , \quad \mathbf{J}_5^{(\mathrm{B})} = \frac{\alpha}{2\pi^2}\mu\mathbf{B}, \tag{17.68}$$

where $\mu_5 = (\mu_{\mathrm{L}} - \mu_{\mathrm{R}})/2$ and $\mu = (\mu_{\mathrm{L}} + \mu_{\mathrm{R}})/2$ are the chiral and the electric chemical potentials, respectively.

The anomalous Hall effect, which is expected to occur in a Weyl semimetal with broken time-reversal (TR) symmetry, is described by the **b**-dependent terms in (17.66) and (17.67). In addition, the b_0-dependent term that arises in Weyl semimetals with broken inversion symmetry, describes only one part of the celebrated chiral magnetic effect, namely, the generation of an electric current driven by an applied magnetic field. The second part is given by $\mathbf{J}^{(\mathrm{B})}$ in (17.68), which arises from an imbalance between chemical potentials of right- and left-handed fermions. The total contribution to the chiral magnetic effect is thus given by $\mathbf{J}_{\mathrm{CME}} = \frac{\alpha}{2\pi^2}\,(\mu_5 - b_0)\,\mathbf{B}$, that vanishes for $b_0 = \mu_5$ in which case the WSM is said to be at the equilibrium state [92]. The electric current $\mathbf{J}_5^B$ in (17.68) is identified as the chiral separation effect, which vanishes for $\mu = 0$, condition that defines the neutrality point [92].

17.6.1 Electric Charge Near a Weyl Semimetal

Recent publications have tackled a number of physical effects on the basis of the above theory. Among them we find the magneto-optical Faraday and Kerr rotations [93] and the Casimir effect [94], as well as the appearance of plasmon polaritons [95] and helicons [96] at the sample's surface. Here, inspired by the image magnetic monopole effect of topological insulators [33, 45, 97], we shall briefly discuss the problem of a pointlike electric charge near the surface of a topological WSM in the equilibrium state and at the neutrality point. This means that the material's response will be a direct consequence of the anomalous Hall effect in the bulk. Charge neutrality is not an unrealistic assumption for WSMs, since it can be attained under specific circumstances, as shown both theoretically and experimentally in [98].

Let us consider a topological Weyl semimetal with a pair of nodes separated along the k_z-direction in the bulk BZ occupying the half-space $z < 0$. The region $z > 0$ is occupied by a dielectric fluid. An electric charge is brought near the surface that does not support Fermi-arc electronic states, in this case the xy-plane for $\mathbf{b} = b\hat{\mathbf{e}}_z$. Neglecting all frequency dependence on the conductivities (since we deal with a static problem), the electromagnetic response of the WSM is fully captured by (17.66) and (17.67), with $b_0 = \mu_5$ and $\mu = 0$. Since $\theta(z = 0) = 0$, there are no surface currents, and the resulting material is just a bulk Hall medium with current responses given by the transverse Hall conductivity

$$\sigma_{xy} = \frac{e^2 b}{2\pi^2 \hbar}. \tag{17.69}$$

Due to the gauge invariance of the theory, we can introduce the electromagnetic potentials as usual: $\mathbf{E} = -\nabla\Phi$ and $\mathbf{B} = \nabla \times \mathbf{A}$. In the Coulomb gauge $\nabla \cdot \mathbf{A} = 0$, for a pointlike electric charge of strength q at $\mathbf{r}' = z'\hat{\mathbf{e}}_z$ with $z' > 0$ (that is the charge lies in the dielectric fluid), the electromagnetic potentials satisfy the coupled equations of motion

$$-\nabla \cdot [\epsilon(z)\nabla\Phi] + \frac{4\pi}{c}\sigma_{xy}(z)\,\hat{\mathbf{e}}_z \cdot \nabla \times \mathbf{A} = 4\pi q \delta(z - z'), \tag{17.70}$$

$$-\nabla^2 \mathbf{A} + \frac{4\pi}{c}\sigma_{xy}(z)\,\hat{\mathbf{e}}_z \times \nabla\Phi = 0, \tag{17.71}$$

where $\sigma_{xy}(z) = \sigma_{xy} H(-z)$ is the bulk Hall conductivity and $\epsilon(z) = \epsilon_1 H(-z) + \epsilon_2 H(z)$ is the static permittivity of the system. The differential equations (17.70) and (17.71), along with the appropriate boundary conditions at the interface $z = 0$ and at the singular point $z = z'$, constitute a complete boundary value problem, which can be solved with standard techniques of electromagnetism [42]. The solution is simple, but not straightforward [99]. On the one hand, the final result for the electrostatic potential beneath the surface is

$$\Phi_{z<0} = 2q \int_0^\infty \frac{(\lambda_+ + k)\cos(\lambda_- z) + \lambda_- \sin(\lambda_- z)}{\epsilon_1\left(\lambda_+^2 + \lambda_-^2\right) + \epsilon_2 k^2 + k\lambda_+(\epsilon_1 + \epsilon_2)} k J_0(k\rho) e^{\lambda_+ z - k z'} dk, \tag{17.72}$$

and, above the surface, we find

$$\Phi_{z>0} = \frac{q}{\epsilon_2}\frac{1}{\sqrt{\rho^2 + (z - z')^2}} + \frac{q}{\epsilon_2}\frac{\epsilon_2 - \epsilon_1}{\epsilon_2 + \epsilon_1}\frac{1}{\sqrt{\rho^2 + (z + z')^2}} - \frac{2q\epsilon_1}{\epsilon_1 + \epsilon_2}\int_0^\infty \frac{\lambda_+^2 + \lambda_-^2 - k^2}{\epsilon_1\left(\lambda_+^2 + \lambda_-^2\right) + \epsilon_2 k^2 + k\lambda_+(\epsilon_1 + \epsilon_2)} J_0(k\rho) e^{-k(z+z')} dk. \tag{17.73}$$

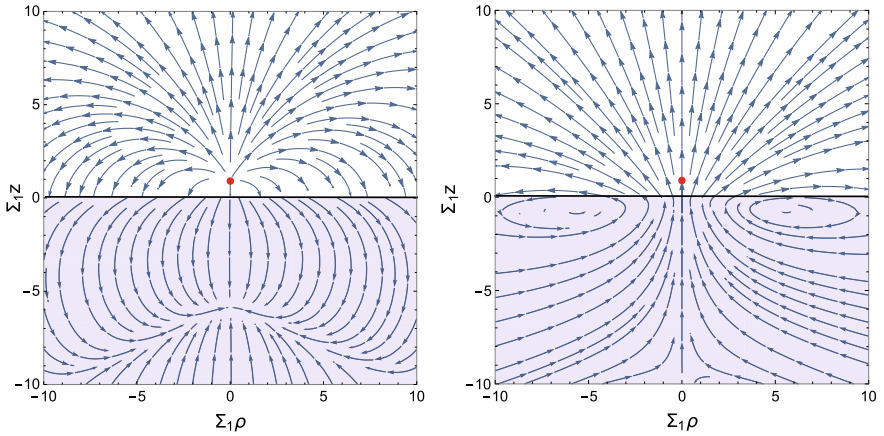

Fig. 17.5 Illustration of the electric (left) and magnetic (right) fields (in units of $q\Sigma^2$), as a function of Σz and $\Sigma\rho$, induced by an electric charge of strength q at $z' = 1/\Sigma$ (marked with the red sphere) above the WSM TaAs (marked with the blue shaded region), (adapted from [99])

In these expressions $\lambda_{\pm}^2 = (k/2)\left[\sqrt{k^2 + \Sigma^2} \pm k\right]$, $\Sigma = 4\pi\sigma_{xy}/(c\sqrt{\epsilon_1})$, $\rho^2 = x^2 + y^2$ and J_n is the nth order Bessel function of the first kind. We observe that in the dielectric fluid, the electric potential can be interpreted as due to the original electric charge of strength q at z', an image electric charge of strength $q(\epsilon_2 - \epsilon_1)/(\epsilon_2 + \epsilon_1)$ at $-z'$, and an additional term arising from the nontrivial topology of the WSM. Inside the material, the electric potential has no simple interpretation. However, as evidenced by the exponential term in (17.72), it is attenuated inside the WSM due to the metallic character of the material. This can also be seen in the limit $\epsilon_1 \to \infty$, for which $\Phi_{z<0} = 0$, as in a perfect conductor.

The electric field is obtained from the above potentials as $\mathbf{E} = -\nabla\Phi$. The left panel of Fig. 17.5 illustrates the electric field $\mathbf{E}$ (in units of $q\Sigma^2$) generated by an electric charge in vacuum ($\epsilon_2 = 1$) at $z' = 1/\Sigma$ (red sphere) close to the WSM TaAs [100] as a function of the dimensionless coordinates $\Sigma\rho$ and Σz. We observe that the electric field outside the WSM is similar to that generated by the original electric charge, with deviations close to the interface due to the screening of the field inside the material. This behaviour is similar to that produced by an electric charge close to an ordinary metal or a dielectric, but the electric field beneath the surface is more complicated than in these nontopological cases. For example, the electric field within a uniform and isotropic dielectric is a radially directed field (with the charge outside the material as its source); while the field inside an ordinary metal is zero. In the present case, as shown in Fig. 17.5, the electric field is remarkably different as evidenced by the curved field lines inside.

On the other hand, the resulting vector potential beneath the surface is

$$\mathbf{A}_{z<0} = 2q\epsilon_1 \hat{\mathbf{e}}_\varphi \int_0^\infty \frac{\lambda_- \cos(\lambda_- z) - (\lambda_+ + k)\sin(\lambda_- z)}{\epsilon_1\left(\lambda_-^2 + \lambda_+^2\right) + \epsilon_2 k^2 + k\lambda_+(\epsilon_1 + \epsilon_2)} k J_1(k\rho) e^{\lambda_+ z - k z'} dk, \tag{17.74}$$

and, above the surface, we obtain

$$\mathbf{A}_{z>0} = 2q\epsilon_1 \hat{\mathbf{e}}_\varphi \int_0^\infty \frac{\lambda_-}{\epsilon_1\left(\lambda_-^2 + \lambda_+^2\right) + \epsilon_2 k^2 + k\lambda_+(\epsilon_1 + \epsilon_2)} k J_1(k\rho) e^{-k(z+z')} dk. \tag{17.75}$$

The magnetic field is obtained as $\mathbf{B} = \nabla \times \mathbf{A}$. The right panel of Fig. 17.5 shows the magnetic field $\mathbf{B}$ (in units of $q\Sigma^2$) induced by an electric charge in vacuum at $z' = 1/\Sigma$ close to the WSM TaAs as a function of the dimensionless coordinates $\Sigma\rho$ and Σz. We observe that in the present case, the behaviour of the field lines is significantly different from the radially directed field lines appearing when the charge is close to a TI. We will discuss this point later.

The physical origin of the magnetic field is the bulk Hall current circulating around the symmetry axis, $\mathbf{J}_{\text{Hall}} = \sigma_{xy}\left(\hat{\mathbf{e}}_\rho \cdot \mathbf{E}_{z<0}\right)\hat{\mathbf{e}}_\varphi$, which is induced by the in-plane component of the electric field produced by the charge. In this way, each cross section (perpendicular to the symmetry axis) of the bulk Hall current resembles the surface Hall current induced by an electric charge near to a topological insulator. This suggests that a 3D Weyl semimetallic phase can be understood as an infinite number of 2+1 Dirac subsystems (one for each value of z in the bulk) supporting a surface Hall current [100].

Now we go back to the discussion of the behaviour of the magnetic field lines in Fig. 17.5. A close inspection reveals that below the surface of the WSM, centered at the position of the image charge, the $\mathbf{B}$-field lines wind in an axisymmetric way as if about a loop of current, similar to those of a physical magnetic dipole. This suggests that we consider a multipole expansion of the magnetic field and determine the dominant contribution. Still, we recall that the source of the magnetic field is not localized (since $\mathbf{J}_{\text{Hall}}$ is defined in the whole bulk), and hence the standard multipole expansion for localized sources does not necessarily applies. In the far zone, the integral in (17.75) can be approximated in powers of $1/r$. The dominant contributions are

$$\mathbf{A}^{(1)} \approx \frac{3}{32}\frac{q}{\Sigma}\sqrt{\frac{\pi}{2}}\frac{\tan(\theta/2)(13 + 3\cos\theta)}{r^{3/2}}\hat{\mathbf{e}}_\varphi, \qquad \mathbf{A}^{(2)} \approx -\frac{q}{\Sigma}\left(1 + \frac{\epsilon_2}{\epsilon_1}\right)\frac{\sin\theta}{r^2}\hat{\mathbf{e}}_\varphi, \tag{17.76}$$

where θ is the angle from the z-axis to the observation point, i.e. $r\cos\theta = \hat{\mathbf{e}}_z \cdot \mathbf{r}$ and $r = \sqrt{\rho^2 + (z + z')^2}$. We observe that the leading term is a fractional multipole, with no analogue in standard electromagnetism. The measurement of this contribution would be a unique signature of the anomalous Hall effect in the bulk of 3D WSMs. The second term can be successfully compared with the vector potential produced

by a magnetic dipole of strength $m = -(q/\Sigma)(1 + \epsilon_2/\epsilon_1)$ located at the image point $-z'$, thus confirming the qualitative expectation that a magnetic dipole is induced.

17.6.2 Experimental Proposals

Now we discuss two specific fingerprints of the induced magnetic field which could, in principle, be measured.

Angle-resolved measurement

In the static case considered above, the WSM attracts the charge toward the surface in the direction perpendicular to it with a force $\mathbf{F}_e = q\mathbf{E}_{z>0}(\mathbf{r}')$, where $\mathbf{r}' = z'\hat{\mathbf{e}}_z$ is the position of the charge. However, interesting phenomena appear when we consider the dynamics of the external charge. Let us consider, for instance, a steady electron beam drifting at a distance z' above the surface of the WSM. To make our solution still valid, we have to consider the electrons slow enough with respect to the Fermi velocity in the solid, in such a way that the induced polarization and magnetization of the material rearranges infinitely fast. So, besides the electrostatic force $\mathbf{F}_e$, if the charge q moves with a uniform velocity $\mathbf{v}$ above the surface of the WSM, a magnetic force of the form $\mathbf{F}_m = q\frac{\mathbf{v}}{c} \times \mathbf{B}_{z>0}(\mathbf{r}')$ will also act on the charge due to the induced magnetic field. For an electron beam moving along the x-direction (with velocity $\mathbf{v} = v_x\hat{\mathbf{e}}_x$) we find

$$\mathbf{F}_m = -2q^2\epsilon_1(v_x/c)\,\hat{\mathbf{e}}_y \int_0^\infty \frac{k^2\lambda_-\, e^{-2kz'}}{\epsilon_1\left(\lambda_+^2 + \lambda_-^2\right) + \epsilon_2 k^2 + k\lambda_+(\epsilon_1 + \epsilon_2)}dk. \qquad (17.77)$$

Remarkably, this anomalous force is orthogonal to the electrons' motion as well as to the electric contribution $\mathbf{F}_e$, and hence these effects can be distinguished from each other. In fact, the effect of the anomalous force (17.77) on the electrons' motion is a deflection in the y-direction which could, in principle, be measurable. For a rough estimate, we take $v_x \sim 10^7$ cm/s (which is appropriate for the steady electron beam emitted from a low-energy electron gun) [101], $z' \sim 1\,\mu$m and $L \sim 1$ cm for the sample's size. So, for a beam of electrons drifting above the WSM TaAs (for which $\epsilon_1 \sim 6$ and $b \sim 10^9\,\mathrm{m}^{-1}$ [100]), the resulting transverse drift would be $3.2\,\mu$m. This deflection can be easily traced by angle-resolved measurement [101]. If this experiment were carried out with a Dirac semimetal by applying an external magnetic field, instead of a genuine WSM such as the TaAs, the induced magnetic field will be overwhelmed by the external one, and so would its contribution to the Lorentz force on a moving charge. For example, by considering the Dirac semimetal Cd_3As_2 in the presence of a magnetic field of 1T (for which $b = 5 \times 10^8\mathrm{m}^{-1}$ and $\epsilon_1 = 12$), the resulting transverse drift is 10^7 larger than the purely topological contribution, thus making its detection challenging. We then conclude that an angle-resolved measure-

ment is appropriate for experimental realization only if it were possible to consider a genuine WSM, for which no external magnetic field is needed.

Scanning SQUID magnetometry

Scanning SQUID (Superconducting Quantum Interference Device) magnetometry provides an alternative for measuring the induced magnetic field. SQUIDs are very sensitive magnetometers based on superconducting loops containing Josephson junctions, and they are used to measure extremely low magnetic fields (of the order of 5×10^{-18}T [102]). In general terms, these devices measure the magnetic flux through a loop (parallel to the surface) placed at a fixed distance above the material, i.e. $\Phi_{\mathbf{B}} = \int_S \mathbf{B} \cdot d\mathbf{S}$, where S is the surface of the loop.

In the present case, a simple calculation produces $\Phi_{\mathbf{B}}(R, z) = 2\pi R\, \hat{\mathbf{e}}_\varphi \cdot \mathbf{A}_{z>0}(R, z)$, where R is the radius of the loop and $\mathbf{A}_{z>0}$ is given by (17.75). Of course, $\Phi_{\mathbf{B}} = 0$ at $R = 0$. Furthermore, since the magnetic field lines start at the WSM surface and go back again to the surface (see the right panel of Fig. 17.5), we then have $\Phi_{\mathbf{B}} \to 0$ as $R \to \infty$. This behaviour implies the existence of a maximum flux at a critical radius R_c, which can be determined in the usual manner (i.e. by solving $\partial_R \Phi_{\mathbf{B}}|_{R=R_c} = 0$ for R_c). For a numerical estimate of the magnetic flux we consider a charge $q = n_e|e|$ placed at a distance $z' = 1\mu$m above the surface of the WSM TaAs and a SQUID of radius $R = 10\mu$m located at $z = 10\mu$m. We find $\Phi_{\mathbf{B}} \approx 7n_e \times 10^{-14}\text{T} \cdot \text{cm}^2$, which is measurable with present day attainable sensitivities of SQUIDs [102]. One of the key challenges for the experimental detection of this flux profile would be to find a way to fix and localize the charge above the surface.

If this experiment were carried out with a Dirac semimetal instead of a genuine WSM, the required external magnetic field will overwhelm the topological contribution to the total magnetic flux, as before. Nevertheless, in this case it is still possible to disentangle these effects by using the fact that the contribution to the flux produced by the external magnetic field, say $\Phi_{\mathbf{B}}^{\text{ext}}$, is constant in space and time, but not $\Phi_{\mathbf{B}}$. A sensitive magnetometer as the SQUID will be capable to measure small variations of the flux which amounts to eventually measuring the induced electromotive force $\mathcal{E}$ in the loop. Therefore, this allows for isolating the topological contribution, for example, by producing a controlled displacement of the SQUID along the z-axis at speed v_z, namely: $\mathcal{E} = -\frac{d}{dt}\left(\Phi_{\mathbf{B}}^{\text{ext}} + \Phi_{\mathbf{B}}\right) = -v_z \frac{d\Phi_{\mathbf{B}}}{dz}$, where the z-dependence is read-off from (17.75).

17.7 Conclusions

In this chapter we have given an overview as to how the properties of magnetoelectric media associated with topological order, that arise from subtleties in their electronic structure, can be understood as macroscopic optical properties in regards to their electromagnetic response. We have presented the reader with the theoretical framework that allows to describe the electromagnetic response of magnetoelectric media

by means of axion-like extended electrodynamics with a non-dynamical axion field θ. Among the benefits of such effective field theory approach is that we can exploit a Green's function formulation to solve for the electromagnetic fields with rather arbitrary configuration of charges, currents, boundary conditions and/or combination of these. Our tools and techniques have been applied to linear isotropic and homogeneous magnetoelectric media with mild coordinate restrictions that are, however, plausible from an experimental point of view. Other benefit of the GF formulation is that the method can be extended to the case of anisotropic media. To illustrate our tools and techniques, we summarize some previously reported results that include: (i) a detailed assessment of the boundary value problem of axion electrodynamics and the modified boundary conditions for the electromagnetic fields across the magnetoelectric interface; (ii) the application to the case of a topological insulator with planar geometry located between two parallel conducting plates to compute the ensuing modification to the Casimir effect; (iii) as an example on how to extend the formulation beyond the static cases, we review some results showing that this technique can be applied to the case of an electric charge traversing from one magnetoelectric medium to another at a constant speed and perpendicular to the interface between them to reveal that, besides the usual forward-directed Vavilov-Cherenkov emission of radiation, a novel feature due entirely to the magnetoelectric effect is an additional backward-directed radiation, termed reversed Vavilov-Cherenkov radiation. Last (iv) we employ the same approach to study the induced electromagnetic fields due to a static electric charge near the surface of a Weyl semimetal in the equilibrium state and at neutrality point to find that inside the WSM medium the induced electric field is nothing like inside a conductor nor insulator and the induced magnetic field outside the WSM has among its multipole contributions one term that corresponds to a magnetic dipole field, as if below the surface of the WSM the electric charge induced a stack of alternating axisymmetric circulating currents centered at the projection of the electric charge. Two different experimental setups are proposed to measure distinctive characteristics of the induced magnetic field as smoking-gun signals of the magnetoelectric effect in WSM and we argue that these observable signals could be measured given the present-day experimental sensitivities available.

As mentioned in the beginning, the study of topological phases of matter is both a fundamental and technological challenge. We think that with our exposition we contributed in both fronts. Our approach allows to shed lights on the understanding of the interaction of these new states of matter with electromagnetic radiation. At the same time, and as a corollary of our approach, we have provided new means to eventually measure observable signals of the magnetoelectric effect using topological insulators or Weyl semimetals. Though we have provided but a few examples, the generality of the Green's function method paves the way for new proposals to similar ends.

Acknowledgements A.M.R. acknowledges support from DGAPA-UNAM project IA101320. M.C. has been partially supported by UNAB DGID under Grant No. DI-33-17/RG. L.F.U. acknowledges support from DGAPA-UNAM Project No. IN103319. We thank to F.M.D. Pellegrino and A. Santonocito for useful remarks.

References

1. C. Nash, S. Sen, *Topology and Geometry for Physicists* (Academic Press Inc, London, 1983)
2. K. Fujikawa, H. Suzuki, *Path Integrals and Quantum Anomalies* (Clarendon Press, Oxford, 2004)
3. M. Dine, TASI Lectures on the Strong CP Problem. arXiv:0011376 [hep-ph] (2000)
4. D. Birmingham, M. Blau, M. Radowski, G. Thompson, Topological field theory. Phys. Rep. **209**, 129 (1991)
5. M. Kuster, G. Raffelt, B. Beltrán (eds), *Axions: Theory, Cosmology, and Experimental Searches* (*Lecture Notes in Physics* vol 741) (Springer, Berlin, 2008)
6. S. Weinberg, The U(1) problem. Phys. Rev. D **11**, 3583 (1975)
7. G. t'Hooft: Symmetry breaking through Bell-Jackiw anomalies. Phys. Rev. Lett. **37**, 8 (1976)
8. G. t'Hooft, Computation of the quantum effects due to a four-dimensional pseudoparticle. Phys. Rev. D **14**, 3432 (1976)
9. R. Peccei, H. Quinn, CP conservation in the presence of pseudoparticles. Phys. Rev. Lett. **38**, 1440 (1977)
10. R. Peccei, H. Quinn, Constraints imposed by CP conservation in the presence of pseudoparticles. Phys. Rev. D **16**, 1791 (1977)
11. P. Sikivie, Experimental tests of the "Invisible" axion. Phys. Rev. Lett. **51**, 1415 (1983)
12. D. Colladay, V.A. Kostelecký, CPT violation and the standard model. Phys. Rev. D **55**, 6760 (1997)
13. D. Colladay, V.A. Kostelecký, Lorentz-violating extension of the standard model. Phys. Rev. D **58**, 116002 (1998)
14. V.A. Kostelecký, M. Mewes, Signals for Lorentz violation in electrodynamics. Phys. Rev. D **66**, 056005 (2002)
15. V.A. Kostelecký, R. Lehnert, M.J. Perry, Spacetime-varying couplings and Lorentz violation. Phys. Rev. D **68**, 123511 (2003)
16. T.H. O'Dell, *The Electrodynamics of Magneto-Electric Media* (North-Holland, Amsterdam, 1970)
17. L.D. Landau, E.M. Lifshitz, L.P. Pitaevskii, *Electrodynamics of Continuous Media* (*Course of Theoretical Physics* vol 8) (Oxford: Pergamon Press, 1984)
18. E. Plum, J. Zhou, J. Dong, V.A. Fedotov, T. Koschny, C.M. Soukoulis, N.I. Zheludev, Metamaterial with negative index due to chirality. Phys. Rev. B **79**, 035407 (2009)
19. X.-L. Qi, T.L. Hughes, S.-C. Zhang, Topological field theory of time-reversal invariant insulators. Phys. Rev. B **78**, 195424 (2008)
20. X.-L. Qi, S.-C. Zhang, Topological insulators and superconductors. Rev. Mod. Phys. **83**, 1057 (2011)
21. M.Z. Hasan, C.L. Kane, Colloquium: Topological insulators. Rev. Mod. Phys. **82**, 3045 (2010)
22. X.-L. Qi, Field-theory foundations of topological insulators, in *Topological Insulators (Contemporary Concepts of Condensed Matter Science)*, Vol. 6, eds. by M. Franz, L. Molenkamp (Elsevier, Amsterdam, 2013)
23. M.M. Vazifeh, M. Franz, Electromagnetic response of weyl semimetals. Phys. Rev. Lett. **111**, 027201 (2013)
24. N.P. Armitage, E.J. Mele, A. Vishwanath, Weyl and Dirac semimetals in three-dimensional solids. Rev. Mod. Phys. **90**, 015001 (2018)
25. J.D. Jackson, *Classical Electrodynamics* (Wiley, Hoboken NJ, 1999)
26. I.E. Dzyaloshinskii, On the magneto-electrical effect in antiferromagnets. JETP **37**, 881 (1959)
27. J.P. Rivera, A short review of the magnetoelectric effect and related experimental techniques on single phase (multi-) ferroics. Eur. Phys. J. B **71**, 299 (2009)
28. G.L. Klimchtskaya, U. Mohideen, V.M. Mostepanenko, The Casimir force between real materials: experiment and theory. Rev. Mod. Phys. **81**, 1827 (2009)
29. Y.N. Obukhov, F.W. Hehl, Measuring a piecewise constant axion field in classical electrodynamics. Phys. Lett. A **341**, 357 (2005)

30. D.N. Astrov, The magneto-electrical effect in antiferromagnets. JETP **38**, 984 (1960)
31. M. Fiebig, Revival of the magnetoelectric effect. J. Phys. D: Appl. Phys. **38**, R123 (2005)
32. V. Dziom, A. Shuvaev, A. Pimenov, G.V. Astakhov, C. Ames, K. Bendias, J. Böttcher, G. Tkachov, E.M. Hankiewicz, C. Brüne, H. Buhmann, L.W. Molenkamp, Observation of the universal magnetoelectric effect in a 3D topological insulator. Nat. Commun. **8**, 15297 (2017)
33. X.-L. Qi, R. Li, J. Zang, S.-C. Zhang, Inducing a magnetic monopole with topological surface States. Science **323**, 1184 (2009)
34. C. Kim, E. Koh, K. Lee, Janus and multifaced supersymmetric theories. J. High Energy Phys. **0806**, 040 (2008)
35. C. Kim, E. Koh, K. Lee, Janus and multifaced supersymmetric theories II. Phys. Rev. D **79**, 126013 (2009)
36. F. Wilczek, Two applications of axion electrodynamics. Phys. Rev. Lett. **58**, 1799 (1987)
37. L. Huerta, J. Zanelli, Optical properties of a θ vacuum. Phys. Rev. D **85**, 085024 (2012)
38. A. Martín-Ruiz, L.F. Urrutia, Interaction of a hydrogenlike ion with a planar topological insulator. Phys. Rev. A **97**, 022502 (2018)
39. A. Martín-Ruiz, E. Chan-López, Dynamics of a Rydberg hydrogen atom near a topologically insulating surface. Eur. Phys. Lett. **119**, 53001 (2017)
40. A.M. Essin, J.E. Moore, D. Vanderbilt, Magnetoelectric polarizability and axion electrodynamics in crystalline insulators. Phys. Rev. Lett. **102**, 146805 (2009)
41. A. Martín-Ruiz, M. Cambiaso, L.F. Urrutia, The magnetoelectric coupling in electrodynamics. Int. J. Mod. Phys. A **34**, 1941002 (2019)
42. J. Schwinger, L. DeRaad, K. Milton, W. Tsai, *Classical Electrodynamics* (Perseus Books, Advanced Book Program, 1998)
43. A. Martín-Ruiz, M. Cambiaso, L.F. Urrutia, Green's function approach to Chern-Simons extended electrodynamics: An effective theory describing topological insulators. Phys. Rev. D **92**, 125015 (2015)
44. A. Martín-Ruiz, M. Cambiaso, L.F. Urrutia, Electro- and magnetostatics of topological insulators as modeled by planar, spherical, and cylindrical θ boundaries: Green's function approach. Phys. Rev. D **93**, 045022 (2016)
45. A. Martín-Ruiz, M. Cambiaso, L.F. Urrutia, Electromagnetic description of three-dimensional time-reversal invariant ponderable topological insulators. Phys. Rev. D **94**, 085019 (2016)
46. A. Martín-Ruiz, Magnetoelectric effect in cylindrical topological insulators. Phys. Rev. D **98**, 056012 (2018)
47. A. Martín-Ruiz, O. Rodríguez-Tzompantzi, J.R. Maze, L.F. Urrutia, Magnetoelectric effect of a conducting sphere near a planar topological insulator. Phys. Rev. A **100**, 042124 (2019)
48. U. Özgür, Y. Alivov, H. Morkoç, Microwave ferrites, part 2: Passive components and electrical tuning. J. Mater. Sci.: Mater. Electron. **20**, 911 (2009)
49. F. Olyslager, I.V. Lindell, Electromagnetics and exotic media: A quest for the Holy Grail. IEEE Antenna's Propagat. Mag. **44**, 48 (2002)
50. H.B.G. Casimir, On the attraction between two perfectly conducting plates. Proc. K. Ned. Akad. Wet. **51**, 793 (1948)
51. G. Bressi, G. Carugno, R. Onofrio, G. Ruoso, Measurement of the Casimir Force between parallel metallic surfaces. Phys. Rev. Lett. **88**, 041804 (2002)
52. K.A. Milton, *The Casimir Effect: Physical Manifestation of Zero-Point Energy* (World Scientific, Singapore, 2001)
53. M. Bordag, G.L. Klimchitskaya, U. Mohideen, V.M. Mostepanenko, *Advances in Casimir Effect* (Oxford University Press, Great Britain, 2009)
54. L. Fu, C.L. Kane, E.J. Mele, Topological insulators in three dimensions. Phys. Rev. Lett. **98**, 106803 (2007); D. Hsieh, D. Qian, L. Wray, Y. Xia, Y.S. Hor, R.J. Cava, M.Z. Hasan, A topological Dirac insulator in a quantum spin Hall phase. Nature **452**, 970 (2008)
55. L.S. Brown, G.J. Maclay, Vacuum stress between conducting plates: an image solution. Phys. Rev. **184**, 1272 (1969)
56. D. Deutsch, P. Candelas, Boundary effects in quantum field theory. Phys. Rev. D **20**, 3063 (1979)

57. A. Martín-Ruiz, M. Cambiaso, L.F. Urrutia, A Green's function approach to the Casimir effect on topological insulators with planar symmetry. Eur. Phys. Lett. **113**, 60005 (2016)
58. R.M. Cavalcanti, Casimir force on a piston. Phys. Rev. D **69**, 065015 (2004)
59. X. Zhou, J. Zhang, X. Ling, S. Chen, H. Luo, S. Wen, Photonic spin Hall effect in topological insulators. Phys. Rev. A **88**, 053840 (2013)
60. A.G. Grushin, A. Cortijo, Tunable Casimir Repulsion with three-dimensional topological insulators. Phys. Rev. Lett. **106**, 020403 (2011)
61. A.G. Grushin, P. Rodriguez-Lopez, A. Cortijo, Effect of finite temperature and uniaxial anisotropy on the Casimir effect with three-dimensional topological insulators. Phys. Rev. B **84**, 045119 (2011)
62. A. Martín-Ruiz, C.A. Escobar, Casimir effect between ponderable media as modeled by the standard model extension. Phys. Rev. D **94**, 076010 (2016)
63. A. Martín-Ruiz, C.A. Escobar, Local effects of the quantum vacuum in Lorentz-violating electrodynamics. Phys. Rev. D **95**, 036011 (2017)
64. O.J. Franca, L.F. Urrutia, O. Rodríguez-Tzompantzi, Reversed electromagnetic erenkov radiation in naturally existing magnetoelectric media. Phys. Rev. D **99**, 116020 (2019)
65. P.A. Čerenkov: Visible luminescence of pure liquids under the influence of γ-radiation. Dokl. Akad. Nauk SSSR **2**, 451 (1934)
66. S.I. Vavilov, On the possible causes of blue γ-glow of liquids. Dokl. Akad. Nauk SSSR **2**, 457 (1934)
67. I.M. Frank, I.E. Tamm: Coherent visible radiation of fast electrons passing through matter. Dokl. Akad. Nauk. **14**, 107 (1937) [Compt. Rend. (Dokl) **14**, 109 (1937)]
68. V.P. Jelley, Cherenkov radiation and its applications. Br. J. Appl. Phys. **6**, 227 (1955)
69. V.P. Jelley, *Cherenkov Radiation and its Applications* (Pergamon, Oxford, 1958)
70. V.G. Veselago, The electrodynamics of substances with simultaneously negative values of ϵ and μ. Soviet Physics Uspekhi **10**, 509 (1968)
71. J.B. Pendry, A.J. Holden, W.J. Stewart, I. Youngs, Extremely low frequency plasmons in metallic mesostructures. Phys. Rev. Lett. **76**, 4773 (1996)
72. J.B. Pendry, A.J. Holden, D.J. Robbins, W.J. Stewart, Magnetism from conductors and enhanced nonlinear phenomena. IEEE Trans. Microwave Theory Tech. **47**, 2075 (1999)
73. J. Lu, T.M. Grzegorczyk, Y. Zhang, J. Pacheco Jr., B.-I. Wu, J.A. Kong, M. Chen, Čerenkov radiation in materials with negative permittivity and permeability. Opt.Exp. **11**, 723 (2003)
74. C. Luo, M. Ibanescu, S.G. Johnson, J.D. Joannopoulos, Cerenkov radiation in photonic crystals. Science **229**, 368 (2003)
75. Z.Y. Duan, B.-I. Wu, S. Xi, H.S. Chen, M. Chen, Research progress in reversed Cherenkov radiations in double-negative metamaterials. Prog. Electromagn. Res. **90**, 75 (2009)
76. S. Xi, H. Chen, T. Jiang, L. Ran, J. Huangfu, B.-I. Wu, J.A. Kong, M. Chen, Experimental verification of reversed Cherenkov radiation in left-handed metamaterial. Phys. Rev. Lett. **103**, 194801 (2009)
77. H. Chen, M. Chen, Flipping photons backward: reversed Cherenkov radiation. Materials Today **14**, 34 (2011)
78. Z. Duan, X. Tang, Z. Wang, Y. Zhang, X. Chen, M. Chen, Y. Gong, Observation of the reversed Cherenkov radiation. Nat. Commun. **8**, 14901 (2017)
79. J. Tao, Q.J. Wang, J. Zhang, Y. Luo, Reverse surface-polariton Cherenkov radiation. Sci. Rep. **6**, 30704 (2016)
80. R.A. Shelby, D.R. Smith, S. Schultz, Experimental verification of a negative index of refraction. Science **292**, 77 (2001)
81. S. Smirnov, Cherenkov sound on a surface of a topological insulator. Phys. Rev. B **88**, 205301 (2013)
82. S. Smirnov, Asymmetric Cherenkov acoustic reverse in topological insulators. Phys. Rev. B **90**, 125305 (2014)
83. W.C. Chew, *Waves and Fields in Inhomogenous Media* (IEEE, New York, 1990)
84. W.C. Chew, A quick way to approximate a Sommerfeld-Weyl-type integral (antenna far-field radiation). IEEE Trans. Antenas Propag. **36**, 1654 (1988)

85. L. Mandel, E. Wolf, *Optical Coherence and Quantum Optics* (Cambridge University Press, Cambridge, England, 1995)
86. A. Sommerfeld, *Partial Differential Equations in Physics* (Academic Press, New York, 1964)
87. J. Schwinger, L. DeRaad and K. Milton: Casimir effect in dielectrics. Ann. Phys. (N.Y.) **115**, 1 (1978)
88. W.K.H. Panofsky, M. Phillips, *Classical Electricity and Magnetism*, 2nd edn. (Addison-Wesley, Reading, MA, 1962)
89. A.A. Zyuzin, A.A. Burkov, Topological response in Weyl semimetals and the chiral anomaly. Phys. Rev. B **86**, 115133 (2012)
90. A.A. Zyuzin, S. Wu, A.A. Burkov, Weyl semimetal with broken time reversal and inversion symmetries. Phys. Rev. B **85**, 165110 (2012)
91. P. Goswami, S. Tewari, Axionic field theory of (3+ 1)-dimensional Weyl semimetals. Phys. Rev. B **88**, 245107 (2013)
92. K. Landsteiner, Notes on anomaly induced transport. Acta Phys. Pol. B **47**, 2617 (2016)
93. M. Kargarian, M. Randeria, N. Trivedi, Theory of Kerr and Faraday rotations and linear dichroism in Topological Weyl Semimetals. Sci. Rep. **5**, 12683 (2015)
94. J.H. Wilson, A.A. Allocca, V. Galitski, Repulsive Casimir force between Weyl semimetals. Phys. Rev. B **91**, 235115 (2015)
95. J. Hofmann, S.D. Sarma, Surface plasmon polaritons in topological Weyl semimetals Phys. Rev. B **93**, 241402(R) (2016)
96. F.M.D. Pellegrino, M.I. Katsnelson, M. Polini, Helicons in Weyl semimetals. Phys. Rev. B **92**, 201407(R) (2015)
97. A. Karch, Electric-magnetic duality and topological insulators. Phys. Rev. Lett. **103**, 171601 (2009)
98. J.-R. Soh, F. de Juan, M.G. Vergniory, N.B.M. Schröter, M.C. Rahn, D.Y. Yan, J. Jiang, M. Bristow, P. Reiss, J.N. Blandy, Y.F. Guo, Y.G. Shi, T.K. Kim, A. McCollam, S.H. Simon, Y. Chen, A.I. Coldea, A.T. Boothroyd, Ideal Weyl semimetal induced by magnetic exchange. Phys. Rev. B **100**, 201102(R) (2019)
99. A. Martín-Ruiz, M. Cambiaso, L.F. Urrutia, Electromagnetic fields induced by an electric charge near a Weyl semimetal. Phys. Rev. B **99**, 155142 (2019)
100. S.-M. Huang, S.-Y. Xu, I. Belopolski, C.-C. Lee, G. Chang, B. Wang, N. Alidoust, G. Bian, M. Neupane, C. Zhang, S. Jia, A. Bansil, H. Lin, M.Z. Hasan, A Weyl Fermion semimetal with surface Fermi arcs in the transition metal monopnictide TaAs class. Nat. Commun. **6**, 7373 (2015)
101. J. Zang, N. Nagaosa, Monopole current and unconventional Hall response on a topological insulator. Phys. Rev. B **81**, 245125 (2010)
102. J.C. Allred, R.N. Lyman, T.W. Kornack, M.V. Romalis, High-sensitivity atomic magnetometer unaffected by spin-exchange relaxation. Phys. Rev. Lett. **89**, 130801 (2002)